Chapter 4
Plates

Plates are one of the most fundamental structural elements which are widely used in a variety of engineering applications. A plate can be defined as a solid body bounded by two parallel flat surfaces having two dimensions relatively greater than the other one (thickness). It can also be viewed as a special case of shells with zero curvature (infinite radii of curvature). The vibration of plates is an old topic and a lot of books, papers and reports have already been published in the past decades. In 1969, A.W. Leissa published an excellent monograph titled *Vibration of Plates*, in which theoretical and experimental results of approximately 500 research papers and reports were presented. Most 90 % of this book considers the homogeneous thin plates. A plate is typically considered to be thin when the ratio of its thickness to representative lateral dimension is less than 1/20 (Leissa 1969; Qatu 2004). As pointed by Leissa (Liew et al. 1998), the classical thin plate theory (CPT) permits one to obtain a fundamental frequency with good accuracy. However, the higher frequencies of a plate with thickness ratio of 1/20, determined by thin plate theory, will not be accurate. It will be somewhat too high. The inaccuracies can be largely eliminated by use of the shear deformation plate theories (SDPTs) for they include both shear deformation and rotary inertia due to rotations. Liew et al. (1998) presented a book deal with thick isotropic plates using the *p*-version Ritz method.

Plates can be rectangular, circular, annular, sectorial, elliptical, triangular, trapezoidal and of other shapes. Chakraverty (2009) analyzed vibrations of plates of various shapes and classical boundary conditions by using the boundary characteristic orthogonal polynomials with the Ritz method. The homogeneous thin plates are the subject of Chakraverty's work as well. With the development of new industries and modern processes, laminated plates composed of composite laminas are extensively used in many fields of modern engineering practices such as space vehicles, civil constructions and deep-sea engineering equipments. Laminated plates are treated by various studies and books. The development of research on this subject has been well documented in several monographs respectively by Qatu (2004), Reddy (2003), Carrera et al. (2011), Ye (2003), and review or survey articles (Carrera 2002, 2003; Liew et al. 2011).

G. Jin et al., *Structural Vibration*, DOI 10.1007/978-3-662-46364-2_4

This chapter considers vibrations of laminated plates with various shapes and general boundary conditions. The fundamental equations of shells in the framework of CST and SDST described in Chap. 1 will be specialized to those of plates by setting the curvatures to zero. We will begin with the fundamental equations of rectangular plates, followed by vibration results of laminated rectangular plates with general boundary conditions. Strain-displacement relations, force and moment resultants, energy functions, governing equations and boundary conditions are derived and shown for both theories. On the basis of SDPT, numerous natural frequencies and mode shapes are presented for laminated rectangular plates with different boundary conditions, lamination schemes and geometry parameters by using the modified Fourier series and weak form solution procedure (see, Chap. 2) because previous studies showed that convergence of solutions with weak form solution procedure is faster (Table 3.3). Effects of boundary conditions, geometry parameters and material properties are studied as well. Vibration of sectorial, annular and circular plates will then be treated in the later sections of this chapter.

4.1 Fundamental Equations of Thin Laminated Rectangular Plates

As shown in Fig. 4.1, a rectangular laminated plate with length a, width b and total thickness of h is selected as the analysis model. To describe the plate clearly, we introduce the following coordinate system: the x-coordinate is taken along the length of the plate, and y- and z-coordinates are taken along the width and the thickness directions, respectively. The middle surface displacements of the plate in the x, y and z directions are denoted by u, v and w, respectively. The laminated rectangular plate is assumed to be composed of N_L composite layers. Consider the laminated rectangular plate and its rectangular coordinate system in Fig. 4.1, the coordinates, characteristics of the Lamé parameters and radii of curvatures are: $\alpha = x$, $\beta = y$, $A = 1$, $B = 1$, $R_\alpha = \infty$, $R_\beta = \infty$.

Fundamental equations of thin laminated rectangular plates are presented in this section by substituting their geometry parameters into those of general thin laminated shell equations.

4.1.1 Kinematic Relations

Based on the assumptions of Kirchhoff, the displacement field of thin rectangular plates is restricted to the following linear relationships (see Fig. 4.2, Reddy (2003)):

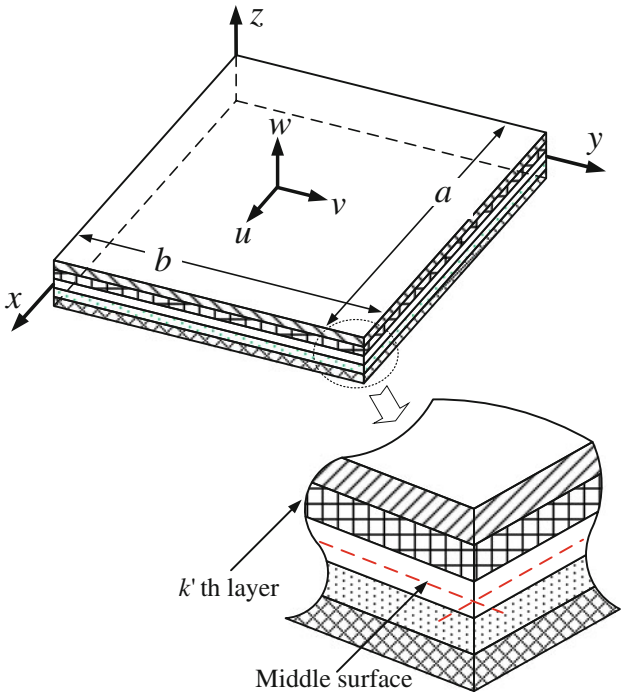

Fig. 4.1 Laminated rectangular plates

$$\begin{aligned} U(x,y,z) &= u(x,y) - z\frac{\partial w(x,y)}{\partial x} \\ V(x,y,z) &= v(x,y) - z\frac{\partial w(x,y)}{\partial y} \\ W(x,y,z) &= w(x,y) \end{aligned} \tag{4.1}$$

where u, v and w are the middle surface displacements. Letting $\alpha = x$, $\beta = y$, $A = B$=1 and $R_\alpha = R_\beta = \infty$, the strain-displacement relations of rectangular plates can be obtained from Eqs. (1.6) and (1.7) as

$$\begin{aligned} \varepsilon_x &= \varepsilon_x^0 + z\chi_x \\ \varepsilon_y &= \varepsilon_y^0 + z\chi_y \\ \gamma_{xy} &= \gamma_{xy}^0 + z\chi_{xy} \end{aligned} \tag{4.2}$$

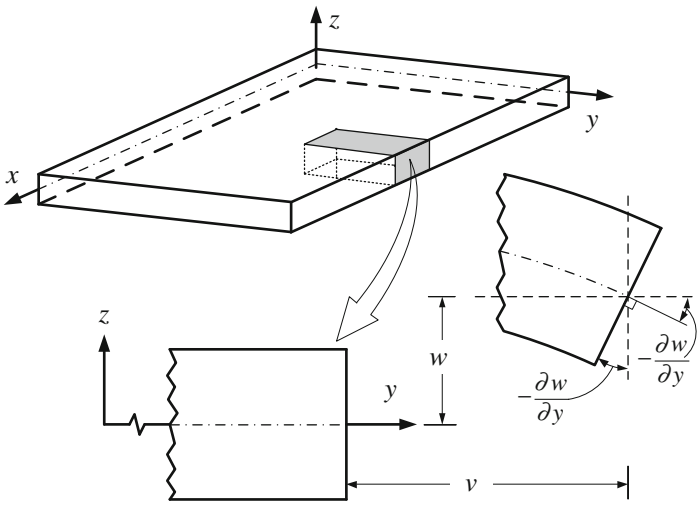

Fig. 4.2 Undeformed and deformed geometries of an edge of a plate under the Kirchhoff assumption (Reddy 2003)

where

$$\begin{aligned} \varepsilon_x^0 &= \frac{\partial u}{\partial x}, & \chi_x &= -\frac{\partial^2 w}{\partial x^2} \\ \varepsilon_y^0 &= \frac{\partial v}{\partial y}, & \chi_y &= -\frac{\partial^2 w}{\partial y^2} \\ \gamma_{xy}^0 &= \frac{\partial v}{\partial x} + \frac{\partial u}{\partial y}, & \chi_{xy} &= -2\frac{\partial^2 w}{\partial x \partial y} \end{aligned} \tag{4.3}$$

4.1.2 Stress-Strain Relations and Stress Resultants

According to Hooke's law, the corresponding stresses in the k'th layer of the plate are written as:

$$\begin{Bmatrix} \sigma_x \\ \sigma_y \\ \tau_{yz} \end{Bmatrix}_k = \begin{bmatrix} \overline{Q_{11}^k} & \overline{Q_{12}^k} & \overline{Q_{16}^k} \\ \overline{Q_{12}^k} & \overline{Q_{22}^k} & \overline{Q_{26}^k} \\ \overline{Q_{16}^k} & \overline{Q_{26}^k} & \overline{Q_{66}^k} \end{bmatrix} \begin{Bmatrix} \varepsilon_x \\ \varepsilon_y \\ \gamma_{xy} \end{Bmatrix}_k \tag{4.4}$$

The lamina stiffness coefficients $\overline{Q_{ij}^k}(i, j = 1, 2, 6)$ can be written as in Eq. (1.9).

Then, the force and moment resultants are obtained by carrying the integration of stresses over the cross-section:

$$\begin{aligned}[N_x \quad N_y \quad N_{xy}] &= \int_{-h/2}^{h/2} [\sigma_x \quad \sigma_y \quad \tau_{xy}]dz \\ [M_x \quad M_y \quad M_{xy}] &= \int_{-h/2}^{h/2} [\sigma_x \quad \sigma_y \quad \tau_{xy}]zdz\end{aligned} \tag{4.5}$$

Performing the integration operation in Eq. (4.5) yields

$$\begin{bmatrix} N_x \\ N_y \\ N_{xy} \\ M_x \\ M_y \\ M_{xy} \end{bmatrix} = \begin{bmatrix} A_{11} & A_{12} & A_{16} & B_{11} & B_{12} & B_{16} \\ A_{12} & A_{22} & A_{26} & B_{12} & B_{22} & B_{26} \\ A_{16} & A_{26} & A_{66} & B_{16} & B_{26} & B_{66} \\ B_{11} & B_{12} & B_{16} & D_{11} & D_{12} & D_{16} \\ B_{12} & B_{22} & B_{26} & D_{12} & D_{22} & D_{26} \\ B_{16} & B_{26} & B_{66} & D_{16} & D_{26} & D_{66} \end{bmatrix} \begin{bmatrix} \varepsilon_x^0 \\ \varepsilon_y^0 \\ \gamma_{xy}^0 \\ \chi_x \\ \chi_y \\ \chi_{xy} \end{bmatrix} \tag{4.6}$$

where N_x, N_y and N_{xy} are the normal and shear force resultants and M_x, M_y, M_{xy} denote the bending and twisting moment resultants. A_{ij}, B_{ij}, and D_{ij} are the stiffness coefficients arising from the piecewise integration over the plate thickness, they can be written as in Eq. (1.15).

In comparing to homogeneous thin plates, there exist some fundamental differences in the equations of generally thin laminated plates. The most important difference is that the transverse vibration is coupled with in-plane vibration for generally laminated plates. When a laminated plate is symmetrically laminated with respect to the middle surface, the constants B_{ij} equal to zero and the in-plane vibration is then decoupled from the transverse vibration, which will sufficiently reduce the complexity of the stress-strain relations, energy functions, governing equations and boundary condition equations of the plate.

4.1.3 Energy Functions

The strain energy (U_s) of thin laminated rectangular plates during vibration can be written as:

$$U_s = \frac{1}{2}\int_0^a \int_0^b \begin{Bmatrix} N_x\varepsilon_x^0 + N_y\varepsilon_y^0 + N_{xy}\gamma_{xy}^0 \\ +M_x\chi_x + M_y\chi_y + M_{xy}\chi_{xy} \end{Bmatrix} dxdy \tag{4.7}$$

Substituting Eqs. (4.3) and (4.6) into Eq. (4.7), the strain energy of the thin laminated plates can be rewritten in terms of displacements as:

$$
\begin{aligned}
U_s = \frac{1}{2}\int_0^a\int_0^b &\left\{\begin{array}{l} A_{11}\left(\frac{\partial u}{\partial x}\right)^2 + 2A_{12}\left(\frac{\partial v}{\partial y}\right)\left(\frac{\partial u}{\partial x}\right) + 2A_{16}\left(\frac{\partial v}{\partial x}+\frac{\partial u}{\partial y}\right)\left(\frac{\partial u}{\partial x}\right) \\ +A_{22}\left(\frac{\partial v}{\partial y}\right)^2 + 2A_{26}\left(\frac{\partial v}{\partial x}+\frac{\partial u}{\partial y}\right)\left(\frac{\partial v}{\partial y}\right) + A_{66}\left(\frac{\partial v}{\partial x}+\frac{\partial u}{\partial y}\right)^2 \end{array}\right\} dydx \\
-\int_0^a\int_0^b &\left\{\begin{array}{l} B_{11}\left(\frac{\partial^2 w}{\partial x^2}\right)\left(\frac{\partial u}{\partial x}\right) + B_{12}\left(\frac{\partial^2 w}{\partial y^2}\right)\left(\frac{\partial u}{\partial x}\right) + 2B_{16}\left(\frac{\partial^2 w}{\partial x\partial y}\right)\left(\frac{\partial u}{\partial x}\right) \\ +B_{12}\left(\frac{\partial^2 w}{\partial x^2}\right)\left(\frac{\partial v}{\partial y}\right) + B_{22}\left(\frac{\partial^2 w}{\partial y^2}\right)\left(\frac{\partial v}{\partial y}\right) + 2B_{26}\left(\frac{\partial^2 w}{\partial x\partial y}\right)\left(\frac{\partial v}{\partial y}\right) \\ +\left(B_{16}\left(\frac{\partial^2 w}{\partial x^2}\right) + B_{26}\left(\frac{\partial^2 w}{\partial y^2}\right) + 2B_{66}\left(\frac{\partial^2 w}{\partial x\partial y}\right)\right)\left(\frac{\partial v}{\partial x}+\frac{\partial u}{\partial y}\right) \end{array}\right\} dydx \\
+\frac{1}{2}\int_0^a\int_0^b &\left\{\begin{array}{l} D_{11}\left(\frac{\partial^2 w}{\partial x^2}\right)^2 + 2D_{12}\left(\frac{\partial^2 w}{\partial y^2}\right)\left(\frac{\partial^2 w}{\partial x^2}\right) + 4D_{16}\left(\frac{\partial^2 w}{\partial x\partial y}\right)\left(\frac{\partial^2 w}{\partial x^2}\right) \\ +D_{22}\left(\frac{\partial^2 w}{\partial y^2}\right)^2 + 4D_{26}\left(\frac{\partial^2 w}{\partial x\partial y}\right)\left(\frac{\partial^2 w}{\partial y^2}\right) + 4D_{66}\left(\frac{\partial^2 w}{\partial x\partial y}\right)^2 \end{array}\right\} dydx
\end{aligned}
\tag{4.8}
$$

The corresponding kinetic energy (T) is:

$$
T = \frac{1}{2}\int_0^a\int_0^b I_0\left\{\left(\frac{\partial u}{\partial t}\right)^2 + \left(\frac{\partial v}{\partial t}\right)^2 + \left(\frac{\partial w}{\partial t}\right)^2\right\} dxdy \tag{4.9}
$$

where the inertia term I_0 is given as in Eq. (1.19). The external work (W_e) is expressed as:

$$
W_e = \int_0^a\int_0^b \left\{q_x u + q_y v + q_z w\right\} dxdy \tag{4.10}
$$

where q_x, q_y and q_z are the external loads in the x, y and z directions, respectively.

As described in Sect. 1.2.3, the general boundary conditions of a plate are implemented by using the artificial spring boundary technique. Specifically, symbols k_ψ^u, k_ψ^v, k_ψ^w and K_ψ^w ($\psi = x0$, $y0$, $x1$ and $y1$) are used to indicate the stiffness of the boundary springs at the boundaries $x = 0$, $y = 0$, $x = a$ and $y = b$, respectively. Therefore, the deformation strain energy about the boundary springs (U_{sp}) is defined as (Fig. 4.3):

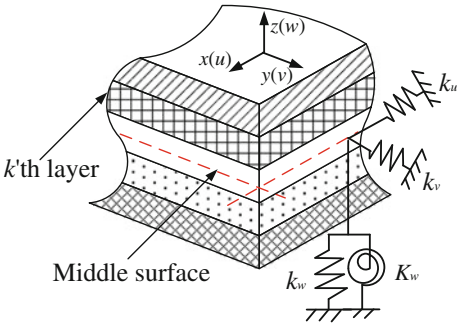

Fig. 4.3 Boundary conditions of thin laminated rectangular plates

$$
\begin{aligned}
U_{sp} = & \frac{1}{2}\int_0^b \left\{ \begin{array}{l} \left[k_{x0}^u u^2 + k_{x0}^v v^2 + k_{x0}^w w^2 + K_{x0}^w(\partial w/\partial x)\right]|_{x=0} \\ +\left[k_{x1}^u u^2 + k_{x1}^v v^2 + k_{x1}^w w^2 + K_{x1}^w(\partial w/\partial x)\right]|_{x=a} \end{array} \right\} dy \\
& + \frac{1}{2}\int_0^a \left\{ \begin{array}{l} \left[k_{y0}^u u^2 + k_{y0}^v v^2 + k_{y0}^w w^2 + K_{y0}^w(\partial w/\partial y)\right]|_{y=0} \\ +\left[k_{y1}^u u^2 + k_{y1}^v v^2 + k_{y1}^w w^2 + K_{y1}^w(\partial w/\partial y)\right]|_{y=b} \end{array} \right\} dx
\end{aligned} \tag{4.11}
$$

4.1.4 Governing Equations and Boundary Conditions

The governing equations and boundary conditions of thin rectangular plates can be obtained by specializing those of thin shells or applying the Hamilton's principle in the same manner as described in Sect. 1.2.4. Substituting $\alpha = x, \beta = y, A = B = 1$ and $R_\alpha = R_\beta = \infty$ into Eq. (1.28) yields following governing equations:

$$
\begin{aligned}
&\frac{\partial N_x}{\partial x} + \frac{\partial N_{xy}}{\partial y} + q_x = I_0 \frac{\partial^2 u}{\partial t^2} \\
&\frac{\partial N_{xy}}{\partial x} + \frac{\partial N_y}{\partial y} + q_y = I_0 \frac{\partial^2 v}{\partial t^2} \\
&\frac{\partial^2 M_x}{\partial x^2} + 2\frac{\partial^2 M_{xy}}{\partial x \partial y} + \frac{\partial^2 M_y}{\partial y^2} + q_z = I_0 \frac{\partial^2 w}{\partial t^2}
\end{aligned} \tag{4.12}
$$

The corresponding boundary conditions of thin laminated plates at boundaries of x = constant are:

$$x = 0: \begin{cases} N_x - k_{x0}^u u = 0 \\ N_{xy} - k_{x0}^v v = 0 \\ Q_x + \frac{\partial M_{xy}}{\partial y} - k_{x0}^w w = 0 \\ -M_x - K_{x0}^w \frac{\partial w}{\partial x} = 0 \end{cases} \quad x = a: \begin{cases} N_x + k_{x1}^u u = 0 \\ N_{xy} + k_{x1}^v v = 0 \\ Q_x + \frac{\partial M_{xy}}{\partial y} + k_{x1}^w w = 0 \\ -M_x + K_{x1}^w \frac{\partial w}{\partial x} = 0 \end{cases} \tag{4.13}$$

Similarly, for boundaries $y = 0$ and $y = b$, the boundary conditions are obtained as:

$$y = 0: \begin{cases} N_{xy} - k_{y0}^u u = 0 \\ N_y - k_{y0}^v v = 0 \\ Q_y + \frac{\partial M_{xy}}{\partial x} - k_{y0}^w w = 0 \\ -M_y - K_{y0}^w \frac{\partial w}{\partial y} = 0 \end{cases} \quad y = b: \begin{cases} N_{xy} + k_{y1}^u u = 0 \\ N_y + k_{y1}^v v = 0 \\ Q_y + \frac{\partial M_{xy}}{\partial x} + k_{y1}^w w = 0 \\ -M_y + K_{y1}^w \frac{\partial w}{\partial y} = 0 \end{cases} \tag{4.14}$$

For generally laminated thin plates, each boundary can exist 12 possible classical boundary conditions. Taking boundaries x = constant for example, the possible combinations for each classical boundary condition are given in Table 4.1.

Table 4.1 Possible classical boundary conditions for generally laminated thin rectangular plates at each boundary of x = constant

Boundary type	Conditions
Free boundary conditions	
F	$N_x = N_{xy} = Q_x + \frac{\partial M_{xy}}{\partial y} = M_x = 0$
F2	$u = N_{xy} = Q_x + \frac{\partial M_{xy}}{\partial y} = M_x = 0$
F3	$N_x = v = Q_x + \frac{\partial M_{xy}}{\partial y} = M_x = 0$
F4	$u = v = Q_x + \frac{\partial M_{xy}}{\partial y} = M_x = 0$
Simply supported boundary conditions	
S	$u = v = w = M_x = 0$
SD	$N_x = v = w = M_x = 0$
S3	$u = N_{xy} = w = M_x = 0$
S4	$N_x = N_{xy} = w = M_x = 0$
Clamped boundary conditions	
C	$u = v = w = \frac{\partial w}{\partial x} = 0$
C2	$N_x = v = w = \frac{\partial w}{\partial x} = 0$
C3	$u = N_{xy} = w = \frac{\partial w}{\partial x} = 0$
C4	$N_x = N_{xy} = w = \frac{\partial w}{\partial x} = 0$

In the framework of artificial spring boundary technique, taking edge $x = 0$ for example, the frequently encountered boundary conditions F, SD, S and C can be readily realized by assigning the stiffness of the boundary springs at proper values as follows:

$$\begin{aligned}
&\text{F: } k_{x0}^{u} = k_{x0}^{v} = k_{x0}^{w} = K_{x0}^{w} = 0 \\
&\text{SD: } k_{x0}^{v} = k_{x0}^{w} = 10^{7}D,\ k_{x0}^{u} = K_{x0}^{w} = 0 \\
&\text{S: } k_{x0}^{u} = k_{x0}^{v} = k_{x0}^{w} = 10^{7}D,\ K_{x0}^{w} = 0 \\
&\text{C: } k_{x0}^{u} = k_{x0}^{v} = k_{x0}^{w} = K_{x0}^{w} = 10^{7}D
\end{aligned} \tag{4.15}$$

where $D = E_1 h^3/12(1-\mu_{12}\,\mu_{21})$ is the flexural stiffness of the plate.

4.2 Fundamental Equations of Thick Laminated Rectangular Plates

This section presents fundamental equations that can be used for thick laminated plates. The treatment that follows is a specialization of shear deformation shell theory (SDST) to laminated plates. For thick plates, the Kirchhoff hypothesis is relaxed by assuming that normals to the undeformed middle surface remain straight but do not normal to the deformed middle surface, see Fig. 4.4 (Reddy 2003). The following equations are referred to as shear deformation plate theory (SDPT).

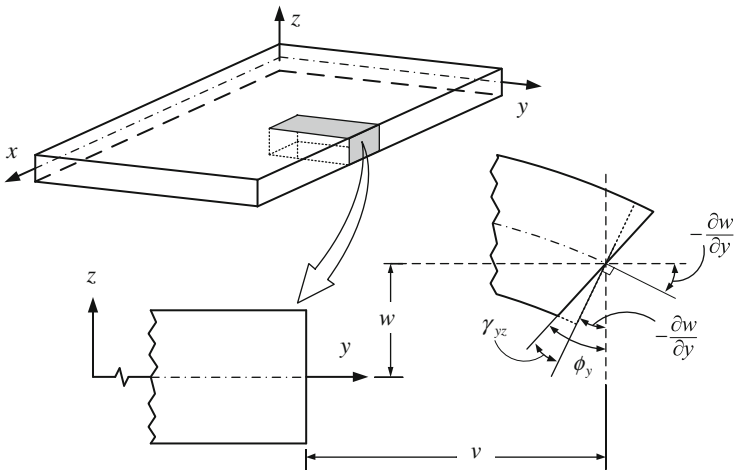

Fig. 4.4 Undeformed and deformed geometries of an edge of a plate including shear deformation

4.2.1 Kinematic Relations

Based on the plate model presented in Fig. 4.1 and the assumptions of the first-order shear deformation theory, the displacement field of thick laminated rectangular plates is of the form

$$\begin{aligned} U(x,y,z) &= u(x,y) + z\phi_x \\ V(x,y,z) &= v(x,y) + z\phi_y \\ W(x,y,z) &= w(x,y) \end{aligned} \tag{4.16}$$

where u, v and w are the middle surface displacements of the plate in the x, y and z directions, respectively; ϕ_x and ϕ_y represent the transverse normal rotations of the reference surface respect to the y and x axes. Specializing Eqs. (1.33) and (1.34) to those of plates, the normal and shear strains at any point of the plate space can be defined in terms of the middle surface strains and curvature changes as:

$$\begin{aligned} \varepsilon_x &= \varepsilon_x^0 + z\chi_x, & \gamma_{xz} &= \gamma_{xz}^0 \\ \varepsilon_y &= \varepsilon_y^0 + z\chi_y, & \gamma_{yz} &= \gamma_{yz}^0 \\ \gamma_{xy} &= \gamma_{xy}^0 + z\chi_{xy} \end{aligned} \tag{4.17}$$

where γ_{xz}^0 and γ_{yz}^0 indicate the transverse shear strains, it is assumed to be constant through the thickness. The middle surface strains and curvature changes are written in terms of middle surface displacements and rotation components as:

$$\begin{aligned} \varepsilon_x^0 &= \frac{\partial u}{\partial x}, & \chi_x &= \frac{\partial \phi_x}{\partial x} \\ \varepsilon_y^0 &= \frac{\partial v}{\partial y}, & \chi_y &= \frac{\partial \phi_y}{\partial y} \\ \gamma_{xy}^0 &= \frac{\partial v}{\partial x} + \frac{\partial u}{\partial y}, & \chi_{xy} &= \frac{\partial \phi_x}{\partial y} + \frac{\partial \phi_y}{\partial x} \\ \gamma_{xz}^0 &= \frac{\partial w}{\partial x} + \phi_x \\ \gamma_{yz}^0 &= \frac{\partial w}{\partial y} + \phi_y \end{aligned} \tag{4.18}$$

4.2.2 Stress-Strain Relations and Stress Resultants

According to Eq. (1.35), the corresponding stress-strain relations in the layer k of a thick laminated rectangular plate are:

$$\begin{Bmatrix} \sigma_x \\ \sigma_y \\ \tau_{yz} \\ \tau_{xz} \\ \tau_{xy} \end{Bmatrix}_k = \begin{bmatrix} \overline{Q_{11}^k} & \overline{Q_{12}^k} & 0 & 0 & \overline{Q_{16}^k} \\ \overline{Q_{12}^k} & \overline{Q_{22}^k} & 0 & 0 & \overline{Q_{26}^k} \\ 0 & 0 & \overline{Q_{44}^k} & \overline{Q_{45}^k} & 0 \\ 0 & 0 & \overline{Q_{45}^k} & \overline{Q_{55}^k} & 0 \\ \overline{Q_{16}^k} & \overline{Q_{26}^k} & 0 & 0 & \overline{Q_{66}^k} \end{bmatrix} \begin{Bmatrix} \varepsilon_x \\ \varepsilon_y \\ \gamma_{yz} \\ \gamma_{xz} \\ \gamma_{xy} \end{Bmatrix}_k \tag{4.19}$$

The force and moment resultants are obtained by integrating the stresses over the plate thickness

$$\begin{aligned} [N_x \quad N_y \quad N_{xy} \quad Q_x \quad Q_y] &= \int_{-h/2}^{h/2} [\sigma_x \quad \sigma_y \quad \tau_{xy} \quad \tau_{xz} \quad \tau_{yz}] dz \\ [M_x \quad M_y \quad M_{xy}] &= \int_{-h/2}^{h/2} [\sigma_x \quad \sigma_y \quad \tau_{xy}] z dz \end{aligned} \tag{4.20}$$

where Q_y and Q_x are the transverse shear force resultants. Carrying out the integration over the thickness, from layer to layer, yields

$$\begin{bmatrix} N_x \\ N_y \\ N_{xy} \\ M_x \\ M_y \\ M_{xy} \end{bmatrix} = \begin{bmatrix} A_{11} & A_{12} & A_{16} & B_{11} & B_{12} & B_{16} \\ A_{12} & A_{22} & A_{26} & B_{12} & B_{22} & B_{26} \\ A_{16} & A_{26} & A_{66} & B_{16} & B_{26} & B_{66} \\ B_{11} & B_{12} & B_{16} & D_{11} & D_{12} & D_{16} \\ B_{12} & B_{22} & B_{26} & D_{12} & D_{22} & D_{26} \\ B_{16} & B_{26} & B_{66} & D_{16} & D_{26} & D_{66} \end{bmatrix} \begin{bmatrix} \varepsilon_x^0 \\ \varepsilon_y^0 \\ \gamma_{xy}^0 \\ \chi_x \\ \chi_y \\ \chi_{xy} \end{bmatrix} \tag{4.21}$$

$$\begin{bmatrix} Q_y \\ Q_x \end{bmatrix} = \begin{bmatrix} A_{44} & A_{45} \\ A_{45} & A_{55} \end{bmatrix} \begin{bmatrix} \gamma_{yz}^0 \\ \gamma_{xz}^0 \end{bmatrix} \tag{4.22}$$

The stiffness coefficients A_{ij}, B_{ij} and D_{ij} are defined as in Eq. (1.43). When a thick rectangular plate is symmetrically laminated with respect to the middle surface, the constants B_{ij} equal to zero, however, the in-plane vibration will not be decoupled from the bending vibration due to the shear deformation.

4.2.3 Energy Functions

The strain energy (U_s) of thick laminated rectangular plates during vibration can be defined in terms of the middle surface strains and curvature changes and stress resultants as

$$U_s = \frac{1}{2}\int_0^a \int_0^b \begin{Bmatrix} N_x\varepsilon_x^0 + N_y\varepsilon_y^0 + N_{xy}\varepsilon_{xy}^0 + M_x\chi_x \\ +M_y\chi_y + M_{xy}\chi_{xy} + Q_y\gamma_{yz} + Q_x\gamma_{xz} \end{Bmatrix} dydx \tag{4.23}$$

Substituting Eqs. (4.18) and (4.21) into Eq. (4.23), the strain energy of the laminated plate can be expressed in terms of displacements (u, v, w) and rotation components (ϕ_x, ϕ_y) as in Eq. (2.84).

The corresponding kinetic energy (T) function is:

$$T = \frac{1}{2}\int_0^a \int_0^b \left\{ \begin{array}{l} I_0\left(\frac{\partial u}{\partial t}\right)^2 + 2I_1\frac{\partial u}{\partial t}\frac{\partial \phi_x}{\partial t} + I_2\left(\frac{\partial \phi_x}{\partial t}\right)^2 + I_0\left(\frac{\partial v}{\partial t}\right)^2 \\ +2I_1\frac{\partial v}{\partial t}\frac{\partial \phi_y}{\partial t} + I_2\left(\frac{\partial \phi_y}{\partial t}\right)^2 + I_0\left(\frac{\partial w}{\partial t}\right)^2 \end{array} \right\} dydx \tag{4.24}$$

The inertia terms are written as in Eq. (1.52). Assuming the distributed external forces q_x, q_y and q_z are in the x, y and z directions, respectively and m_x and m_y represent the external couples in the middle surface, thus, the work done by the external forces and moments is

$$W_e = \int_0^a \int_0^b \{q_x u + q_y v + q_z w + m_x\phi_x + m_y\phi_y\} dydx \tag{4.25}$$

Using the artificial spring boundary technique similar to that described earlier, symbols $k_\psi^u, k_\psi^v, k_\psi^w, K_\psi^x$ and K_ψ^y (ψ = $x0$, $y0$, $x1$ and $y1$) are used to indicate the rigidities (per unit length) of the boundary springs at the boundaries $x = 0$, $y = 0$, $x = a$ and $y = b$, respectively, see Fig. 4.5. Therefore, the deformation strain energy (U_{sp}) stored in the boundary springs during vibration is defined as:

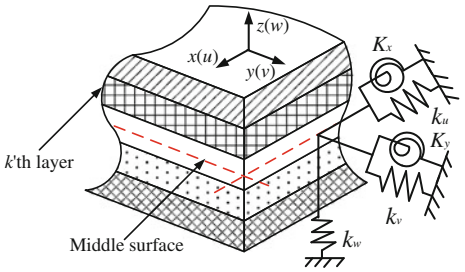

Fig. 4.5 Boundary conditions of a thick laminated rectangular plate

$$U_{sp} = \frac{1}{2}\int_0^b \left\{ \begin{array}{l} \left[k_{x0}^u u^2 + k_{x0}^v v^2 + k_{x0}^w w^2 + K_{x0}^x \phi_x^2 + K_{x0}^y \phi_y^2\right]|_{x=0} \\ + \left[k_{x1}^u u^2 + k_{x1}^v v^2 + k_{x1}^w w^2 + K_{x1}^x \phi_x^2 + K_{x1}^y \phi_y^2\right]|_{x=a} \end{array} \right\} dy \\ + \frac{1}{2}\int_0^a \left\{ \begin{array}{l} \left[k_{y0}^u u^2 + k_{y0}^v v^2 + k_{y0}^w w^2 + K_{y0}^x \phi_x^2 + K_{y0}^y \phi_y^2\right]|_{y=0} \\ + \left[k_{y1}^u u^2 + k_{y1}^v v^2 + k_{y1}^w w^2 + K_{y0}^x \phi_x^2 + K_{y0}^y \phi_y^2\right]|_{y=b} \end{array} \right\} dx \tag{4.26}$$

4.2.4 Governing Equations and Boundary Conditions

Specializing the governing equations and boundary conditions of thick general shells (Eq. (1.59)) to those of thick rectangular plates, we have

$$\begin{aligned} &\frac{\partial N_x}{\partial x} + \frac{\partial N_{xy}}{\partial y} + q_x = I_0 \frac{\partial^2 u}{\partial t^2} + I_1 \frac{\partial^2 \phi_x}{\partial t^2} \\ &\frac{\partial N_{xy}}{\partial x} + \frac{\partial N_y}{\partial y} + q_y = I_0 \frac{\partial^2 v}{\partial t^2} + I_1 \frac{\partial^2 \phi_y}{\partial t^2} \\ &\frac{\partial Q_x}{\partial x} + \frac{\partial Q_y}{\partial y} + q_z = I_0 \frac{\partial^2 w}{\partial t^2} \\ &\frac{\partial M_x}{\partial x} + \frac{\partial M_{xy}}{\partial y} - Q_x + m_x = I_1 \frac{\partial^2 u}{\partial t^2} + I_2 \frac{\partial^2 \phi_x}{\partial t^2} \\ &\frac{\partial M_{xy}}{\partial x} + \frac{\partial M_y}{\partial y} - Q_y + m_y = I_1 \frac{\partial^2 v}{\partial t^2} + I_2 \frac{\partial^2 \phi_y}{\partial t^2} \end{aligned} \tag{4.27}$$

Substituting Eqs. (4.17), (4.18), (4.21) and (4.22) into above equations, the governing equations can be written in terms of displacements. These equations are proved useful when exact solutions are desired. These equations can be written as

$$\left(\begin{bmatrix} L_{11} & L_{12} & L_{13} & L_{14} & L_{15} \\ L_{21} & L_{22} & L_{23} & L_{24} & L_{25} \\ L_{31} & L_{32} & L_{33} & L_{34} & L_{35} \\ L_{41} & L_{42} & L_{43} & L_{44} & L_{45} \\ L_{51} & L_{52} & L_{53} & L_{54} & L_{55} \end{bmatrix} - \omega^2 \begin{bmatrix} M_{11} & 0 & 0 & M_{14} & 0 \\ 0 & M_{22} & 0 & 0 & M_{25} \\ 0 & 0 & M_{33} & 0 & 0 \\ M_{41} & 0 & 0 & M_{44} & 0 \\ 0 & M_{52} & 0 & 0 & M_{55} \end{bmatrix} \right) \begin{bmatrix} u \\ v \\ w \\ \phi_x \\ \phi_y \end{bmatrix} = \begin{bmatrix} -p_x \\ -p_y \\ -p_z \\ -m_x \\ -m_y \end{bmatrix} \tag{4.28}$$

The coefficients of the linear operator L_{ij} and M_{ij} are given as in Eq. (2.49). The general boundary conditions of the plate are:

$$
x{=}0:\begin{cases} N_x - k_{x0}^{u}u = 0 \\ N_{xy} - k_{x0}^{v}v = 0 \\ Q_x - k_{x0}^{w}w = 0 \\ M_x - K_{x0}^{x}\phi_x = 0 \\ M_{xy} - K_{x0}^{y}\phi_y = 0 \end{cases} \quad
x{=}a:\begin{cases} N_x + k_{x1}^{u}u = 0 \\ N_{xy} + k_{x1}^{v}v = 0 \\ Q_x + k_{x1}^{w}w = 0 \\ M_x + K_{x1}^{x}\phi_x = 0 \\ M_{xy} + K_{x1}^{y}\phi_y = 0 \end{cases}
$$

$$
y{=}0:\begin{cases} N_{xy} - k_{y0}^{u}u = 0 \\ N_y - k_{y0}^{v}v = 0 \\ Q_y - k_{y0}^{w}w = 0 \\ M_{xy} - K_{y0}^{x}\phi_x = 0 \\ M_y - K_{y0}^{y}\phi_y = 0 \end{cases} \quad
y{=}b:\begin{cases} N_{xy} + k_{y1}^{u}u = 0 \\ N_y + k_{y1}^{v}v = 0 \\ Q_y + k_{y1}^{w}w = 0 \\ M_{xy} + K_{y1}^{x}\phi_x = 0 \\ M_y + K_{y1}^{y}\phi_y = 0 \end{cases} \tag{4.29}
$$

The classification of the classical boundary conditions shown in Table 1.3 for thick laminated shells is applicable for plates. Taking boundaries x = constant for example, the possible combinations for each classical boundary conditions are given in Table 4.2.

Similarly, in the framework of artificial spring boundary technique, the aforementioned classical boundary conditions can be readily realized by assigning the stiffness of the boundary springs at proper values. Taking edge $x = 0$ for example, the frequently encountered boundary conditions F, SD (shear-diaphragm), S (simply-supported) and C can be defined in terms of boundary spring rigidities as follows:

$$
\begin{aligned}
&\text{F: } k_{x0}^{u} = k_{x0}^{v} = k_{x0}^{w} = K_{x0}^{x} = K_{x0}^{y} = 0 \\
&\text{SD: } k_{x0}^{v} = k_{x0}^{w} = K_{x0}^{y} = 10^7 D,\ k_{x0}^{u} = K_{x0}^{x} = 0 \\
&\text{S: } k_{x0}^{u} = k_{x0}^{v} = k_{x0}^{w} = K_{x0}^{y} = 10^7 D,\ K_{x0}^{x} = 0 \\
&\text{C: } k_{x0}^{u} = k_{x0}^{v} = k_{x0}^{w} = K_{x0}^{x} = K_{x0}^{y} = 10^7 D
\end{aligned} \tag{4.30}
$$

where $D = E_1h^3/12(1\text{-}\mu_{12}\mu_{21})$ is the flexural stiffness of the plate. Figure 4.6 (Ye et al. 2014a) shows the variations of the first three frequency parameters $\Delta\Omega$ versus restraint parameters Γ_λ ($\lambda = u, v, w, x$ and y) of a [0°/90°/0°] laminated plate ($a/b = 1$, $h/a = 0.1$, $E_1/E_2 = 40$, $\mu_{12} = 0.25$, $G_{12} = 0.6E_2$, $G_{13} = 0.6E_2$ and $G_{23} = 0.5E_2$), where $\Delta\Omega$ is defined as the difference of the frequency parameter $\Omega = \omega b^2/\pi^2\sqrt{\rho h/D}$ to that of the elastic restraint parameter $\Gamma_\lambda = 10^{-1}$, namely, $\Delta\Omega = \Omega\ (\Gamma_\lambda) - \Omega\ (10^{-1}D)$. The plates under consideration are completely free at boundaries $y = 0$, $y = b$, and completely clamped at boundary $x = 0$, while at edge $x = a$, the plates are elastically supported by only one group of spring components with stiffness assigned as $\Gamma \times D$. According to Fig. 4.6, we can see that when the restraint parameter Γ is increased from 10^0 to 10^5, the frequency parameters increase rapidly and approach their utmost. Then they remain unchanged when Γ approaches infinity. In such a case, the plate can be deemed as clamped in both ends. Thus, by assigning the stiffness of the entire boundary springs at 10^7D, the completely clamped boundary conditions of a plate can be realized.

Table 4.2 Possible classical boundary conditions for thick rectangular plates at each boundary of x = constant

Boundary type	Conditions
Free boundary conditions	
F	$N_x = N_{xy} = Q_x = M_x = M_{xy} = 0$
F2	$u = N_{xy} = Q_x = M_x = M_{xy} = 0$
F3	$N_x = v = Q_x = M_x = M_{xy} = 0$
F4	$u = v = Q_x = M_x = M_{xy} = 0$
F5	$N_x = N_{xy} = Q_x = M_x = \phi_y = 0$
F6	$u = N_{xy} = Q_x = M_x = \phi_y = 0$
F7	$N_x = v = Q_x = M_x = \phi_y = 0$
F8	$u = v = Q_x = M_x = \phi_y = 0$
Simply supported boundary conditions	
S	$u = v = w = M_x = \phi_y = 0$
SD	$N_x = v = w = M_x = \phi_y = 0$
S3	$u = N_{xy} = w = M_x = \phi_y = 0$
S4	$N_x = N_{xy} = w = M_x = \phi_y = 0$
S5	$u = v = w = M_x = M_{xy} = 0$
S6	$N_x = v = w = M_x = M_{xy} = 0$
S7	$u = N_{xy} = w = M_x = M_{xy} = 0$
S8	$N_x = N_{xy} = w = M_x = M_{xy} = 0$
Clamped boundary conditions	
C	$u = v = w = \phi_x = \phi_y = 0$
C2	$N_x = v = w = \phi_x = \phi_y = 0$
C3	$u = N_{xy} = w = \phi_x = \phi_y = 0$
C4	$N_x = N_{xy} = w = \phi_x = \phi_y = 0$
C5	$u = v = w = \phi_x = M_{xy} = 0$
C6	$N_x = v = w = \phi_x = M_{xy} = 0$
C7	$u = N_{xy} = w = \phi_x = M_{xy} = 0$
C8	$N_x = N_{xy} = w = \phi_x = M_{xy} = 0$

4.3 Vibration of Laminated Rectangular Plates

In this section, we consider free vibration laminated rectangular plates with general boundary conditions. The homogeneous rectangular plates are treated as a special case of the laminated ones in the study. Only solutions in the framework of SDPT are considered in this section. Natural frequencies and mode shapes for thin and thick laminated rectangular plates with different boundary conditions, lamination schemes and geometry parameters are presented. For the sake of simplicity, a four-letter string is employed to represent the boundary condition of a plate, such as FCSSD identify a rectangular plate with edges $x = 0$, $y = 0$, $x = a$, $y = b$ having F, C, S and SD boundary conditions, respectively.

Combining Eqs. (2.49) and (4.28), it is obvious that the displacements and rotation components of laminated rectangular plates in the framework of SDPT are

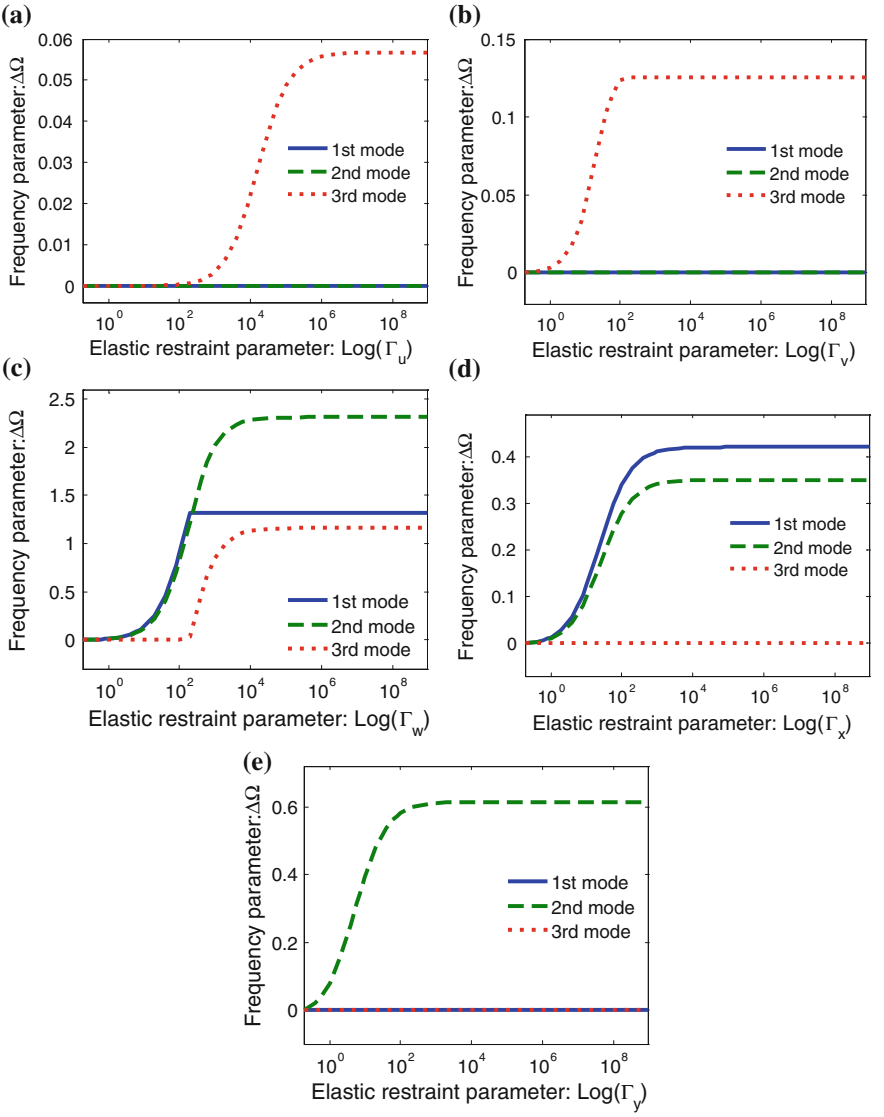

Fig. 4.6 Variation of the frequency parameters $\Delta\Omega$ versus the elastic restraint parameters Γ_λ for a three-layered, [0°/90°/0°] rectangular plate

required to have up to the second derivatives. Therefore, regardless of boundary conditions, each displacement and rotation component of a laminated plate is expanded as a two-dimensional modified Fourier series as:

$$
\begin{aligned}
u(x,y) &= \sum_{m=0}^{M}\sum_{n=0}^{N} A_{mn}\cos\lambda_m x\, cos\lambda_n y + \sum_{l=1}^{2}\sum_{n=0}^{N} a_{ln}P_l(x)\cos\lambda_n y \\
&\quad + \sum_{l=1}^{2}\sum_{m=0}^{M} b_{lm}P_l(y)\cos\lambda_m x \\
v(x,y) &= \sum_{m=0}^{M}\sum_{n=0}^{N} B_{mn}\cos\lambda_m x\, cos\lambda_n y + \sum_{l=1}^{2}\sum_{n=0}^{N} c_{ln}P_l(x)\cos\lambda_n y \\
&\quad + \sum_{l=1}^{2}\sum_{m=0}^{M} d_{lm}P_l(y)\cos\lambda_m x \\
w(x,y) &= \sum_{m=0}^{M}\sum_{n=0}^{N} C_{mn}\cos\lambda_m x\, cos\lambda_n y + \sum_{l=1}^{2}\sum_{n=0}^{N} e_{ln}P_l(x)\cos\lambda_n y \\
&\quad + \sum_{l=1}^{2}\sum_{m=0}^{M} f_{lm}P_l(y)\cos\lambda_m x \\
\phi_x(x,y) &= \sum_{m=0}^{M}\sum_{n=0}^{N} D_{mn}\cos\lambda_m x\cos\lambda_n y + \sum_{l=1}^{2}\sum_{n=0}^{N} g_{ln}P_l(x)\cos\lambda_n y \\
&\quad + \sum_{l=1}^{2}\sum_{m=0}^{M} h_{lm}P_l(y)\cos\lambda_m x \\
\phi_y(x,y) &= \sum_{m=0}^{M}\sum_{n=0}^{N} E_{mn}\cos\lambda_m x\cos\lambda_n y + \sum_{l=1}^{2}\sum_{n=0}^{N} i_{ln}P_l(x)\cos\lambda_n y \\
&\quad + \sum_{l=1}^{2}\sum_{m=0}^{M} j_{lm}P_l(y)\cos\lambda_m x
\end{aligned}
\tag{4.31}
$$

where $\lambda_m = m\pi/a$ and $\lambda_n = n\pi/b$. A_{mn}, B_{mn}, C_{mn}, D_{mn} and E_{mn} are expansion coefficients of the standard cosine Fourier series. a_{ln}, b_{lm}, c_{ln}, d_{lm}, e_{ln}, f_{lm} g_{ln}, h_{lm}, i_{ln} and j_{lm} are the corresponding supplement coefficients. M and N denote the truncation numbers with respect to variables x and y, respectively. $P_l\,(x)$ and $P_l\,(y)$ denote the auxiliary polynomial functions introduced to remove all the discontinuities potentially associated with the first-order derivatives at the boundaries. These auxiliary functions are defined as

$$
P_1(x) = x\left(\frac{x}{a}-1\right)^2 \quad P_2(x) = \frac{x^2}{a}\left(\frac{x}{a}-1\right) \tag{4.32}
$$

$$
P_1(y) = y\left(\frac{y}{b}-1\right)^2 \quad P_2(y) = \frac{y^2}{b}\left(\frac{y}{b}-1\right) \tag{4.33}
$$

The solutions of laminated rectangular plates under consideration can be sought in the strong form solution procedure as described in Sect. 2.1.2. Alternately, all the

expansion coefficients in Eq. (4.31) can be treated equally and independently as the generalized coordinates and solved directly from the Rayleigh–Ritz technique in a fashion similar to that done in Sect. 2.2. Table 3.3 shows that the solutions obtained by the weak form solution procedure (i.e., Ritz technique) converge faster than those of strong form solution procedure, therefore, the weak form solution procedure will be adopted in the following calculation. Unless otherwise stated, the natural frequencies of the considered plates are expressed in the non-dimensional parameters as $\Omega = \omega a^2\sqrt{\rho/E_2h^2}$ and the material properties of the layers are given as: E_2 = 10 GPa, E_1/E_2 = open, μ_{12} = 0.25, $G_{12} = 0.6E_2$, $G_{13} = 0.6E_2$, $G_{23} = 0.5E_2$ and ρ = 1,450 kg/m^3.

4.3.1 Convergence Studies and Result Verification

A moderately thick, symmetrically laminated rectangular plate with completely free boundary condition has been selected to demonstrate the convergence and accuracy of the current method. The material properties and geometrical dimensions of the plate are given as follows: a/b = 3/2, h/a = 0.1, E_1/E_2 = 20, μ_{12} = 0.25, $G_{12} = 0.5E_2$, $G_{13} = 0.5E_2$ and $G_{23} = 0.33E_2$. In Table 4.3 (Ye et al. 2014a), the first six frequency parameters $\Omega = \omega a^2\sqrt{\rho/E_1h^2}$ for the plate with [30°/−30°/−30°/30°] lamination scheme are examined. Results without considering the supplementary terms in the admissible functions are also included in the table. The table shows the proposed method has fast convergence behavior. The maximum discrepancy in the worst case between the 11 × 11 truncated configuration and the 13 × 13 one is less than 0.0013 %. In order to check the model, the present results are also compared with

Table 4.3 Comparison and convergence of the first six frequency parameters $\Omega = \omega a^2\sqrt{\rho/E_1h^2}$ for a completely free, [30°/−30°/−30°/30°] laminated rectangular plate (a/b = 3/2, h/a = 0.1)

Methods	$M \times N$	Mode number					
		1	2	3	4	5	6
Present	11 × 11	2.3449	2.8767	4.9502	5.1610	5.6962	8.4310
	12 × 12	2.3449	2.8767	4.9502	5.1610	5.6962	8.4310
	13 × 13	2.3449	2.8767	4.9502	5.1610	5.6962	8.4310
Present *	11 × 11	0.7499	1.0034	2.2191	2.8797	3.7857	4.2837
	12 × 12	0.7141	0.9565	2.1952	2.7305	3.7630	4.2406
	13 × 13	0.7051	0.9472	2.1472	2.6935	3.6792	4.1875
Frederiksen (1995)	16 × 16	2.3223	2.8745	4.9152	5.0674	5.6589	8.2288
	18 × 18	2.3223	2.8745	4.9152	5.0674	5.6589	8.2288
Messina and Soldatos (1999a)		2.3251	2.8777	4.9458	5.0910	5.6871	8.3580

*Present** Results without considering the supplementary terms in Eq. (4.31)

Table 4.4 Comparison of the frequency parameters $\Omega = \omega b^2/\pi^2\sqrt{\rho/E_2h^2}$ for a thick, [45°/−45°/45°/−45°/45°] laminated plate (a/b = 1, h/a = 0.1, E_1/E_2 = 40)

Boundary conditions	Method	Mode number					
		1	2	3	4	5	6
SSSS	Present	1.8803	3.3763	3.6923	4.9665	5.4801	5.5985
	Karami et al. (2006)	1.8788	3.3776	3.6921	4.9680	5.4834	5.6000
	Wang (1997)	1.8792	3.3776	3.6924	4.9682	5.4835	5.6002
	Liew et al. (2005)	1.8466	3.3774	3.6425	4.9661	5.4348	5.5187
CCCC	Present	2.2855	3.7363	3.9792	5.1777	5.6966	5.8416
	Karami et al. (2006)	2.2857	3.7392	3.9813	5.1799	5.7019	5.8454
	Wang (1997)	2.2857	3.7392	3.9813	5.1800	5.7019	5.8455
	Liew et al. (2005)	2.2785	3.7383	3.9583	5.1836	5.6808	5.8066

data published by Frederiksen (1995) who used Ritz method, Messina and Soldatos (1999a) based on HSDT formulation. From the table, one can see that the present solutions agree very well with the referential results.

To further validate the accuracy and reliability of current solutions, Table 4.4 (Ye et al. 2014a) shows the comparison of the first six frequency parameters $\Omega = \omega b^2/\pi^2\sqrt{\rho/E_2h^2}$ of a thick, [45°/−45°/45°/−45°/45°] laminated plate which was studied by Karami et al. (2006), Liew et al. (2005) and Wang (1997). The material properties and geometrical dimensions used in the investigation are: a/b = 1, h/a = 0.1, E_1/E_2 = 40. The SSSS and CCCC boundary conditions are performed in the comparison. It is observed that the comparison is very good. The discrepancies are negligible and the worst one is less than 1.83 %.

4.3.2 *Laminated Rectangular Plates with Arbitrary Classical Boundary Conditions*

The excellent agreement between the current solutions and those provided by other researchers observed from Tables 4.3 and 4.4 indicate that the proposed method is sufficiently accurate to deal with laminated rectangular plates with arbitrary boundary conditions. It also verified that the definition of the four types of classical boundaries in Eq. (4.30) is appropriate. In this section, laminated rectangular plates with various boundary conditions including the classical restraints and the elastic ones will be studied.

In Table 4.5, the first four non-dimension frequency parameters Ω of a two-layered, angle-ply [45°/−45°] laminated square plate (E_1/E_2 = 40) subjected to five possible combinations of boundary conditions are presented. Four different thickness-length ratios, i.e. h/a = 0.01, 0.05, 0.1 and 0.15, corresponding to thin to thick

Table 4.5 The first four frequency parameters Ω for a [45°/−45°] laminated square plate with various boundary conditions and thickness–length ratios

h/*a*	Mode number	Boundary conditions				
		FFFF	FSFS	FCFC	SSSS	CCCC
0.01	1	7.9118	6.2094	12.320	18.457	23.325
	2	11.467	12.849	17.489	37.712	46.788
	3	14.782	21.385	31.281	37.712	46.788
	4	24.979	28.160	34.054	63.436	73.851
	5	24.979	32.609	41.532	64.007	80.563
0.05	1	7.8140	6.0044	11.703	17.628	21.405
	2	10.964	12.234	16.111	34.803	41.031
	3	14.391	20.220	27.942	34.803	41.031
	4	22.971	26.027	30.872	56.213	61.328
	5	22.971	29.825	36.684	56.379	67.024
0.10	1	7.5763	5.6488	10.480	15.621	17.910
	2	10.176	11.216	13.871	28.893	31.961
	3	13.515	18.065	23.029	28.893	31.961
	4	19.946	22.357	25.207	43.258	44.986
	5	19.946	25.281	29.347	44.388	48.908
0.15	1	7.2469	5.2481	9.1388	13.451	14.794
	2	9.3174	10.121	11.816	23.591	25.081
	3	12.437	15.834	19.078	23.591	25.081
	4	17.088	18.897	20.312	33.556	34.211
	5	17.088	21.168	23.548	35.125	37.055

plates are performed in the calculation. It can be seen from the table that the augmentation of the thickness-length ratio leads to the decrease of the frequency parameters. Then let us consider moderately thick (h/a = 0.05), [0°/90°] and [0°/90°/0°] laminated rectangular (b/a = 2) plates with various anisotropic degrees. In Table 4.6, the first three frequency parameters Ω for the plates with four types of boundary conditions and five different anisotropic degrees, i.e. E_1/E_2 = 1, 5, 10, 20 and 40 are listed, respectively. It can be seen from the table that the frequency parameters increase in general as the anisotropic ratio increases.

In a composite lamina, fibers are the principal load carrying members (Reddy 2003). By appropriately arranging the fiber directions in the layers of a laminated plate, special functional requirements can be satisfied. The influence of fiber orientations on the vibration characteristics of composite laminated plates is investigated. In Fig. 4.7 (Ye et al. 2014a), variation of the lowest four frequency parameters Ω of a three-layered, [0°/ϑ/0°] composite plate with CFFF and CFCF boundary conditions against the fiber direction angle ϑ are depicted, respectively. The geometric and material properties of the layers of the plate are: a/b = 1,

Table 4.6 The first three frequency parameters Ω for [0°/90°] and [0°/90°/0°] laminated rectangular plates with various anisotropic degrees (b/a = 2, h/a = 0.05)

Boundary conditions	E_1/E_2	[0°/90°]			[0°/90°/0°]		
		1	2	3	1	2	3
FFFF	1	1.6186	2.4368	4.4783	1.6186	2.4363	4.4779
	5	2.2796	2.4714	5.4939	1.7283	2.4512	4.7494
	10	2.4895	2.6649	5.6947	1.8618	2.4598	5.1119
	20	2.5122	3.2378	6.0173	2.1036	2.4729	5.4672
	40	2.5380	4.1190	6.5613	2.4927	2.5179	5.6761
SDSDSDSD	1	3.8245	6.2386	10.007	3.8244	6.2378	10.005
	5	4.7235	7.2379	11.887	6.7027	8.3403	11.545
	10	5.3177	7.9484	13.174	9.0302	10.352	13.267
	20	6.2521	9.1169	15.236	12.270	13.351	16.049
	40	7.7320	11.025	18.515	16.547	17.487	20.152
SSSS	1	3.8837	6.3851	10.207	3.8839	6.3851	10.206
	5	5.4240	7.9582	12.629	6.7356	8.4471	11.711
	10	6.7036	9.2081	14.405	9.0538	10.435	13.407
	20	8.5373	11.043	17.090	12.287	13.413	16.158
	40	11.135	13.755	21.157	16.559	17.530	20.232
CCCC	1	7.3712	9.7520	13.697	7.3733	9.7535	13.697
	5	9.6590	12.147	16.906	13.969	15.344	18.173
	10	11.049	13.668	18.954	18.547	19.622	22.041
	20	13.112	15.991	22.086	23.992	24.886	27.090
	40	16.171	19.520	26.832	29.592	30.499	32.762

h/a = 0.1, E_1/E_2 = 40. Many interesting characteristics can be observed from the figures. Firstly, all the figures are symmetrical about ϑ = 90°. From Fig. 4.7a, we can see that there is little variation in the 1st and 2nd mode frequency parameters when ϑ is increased from 0 to 90°. However, for the 3rd mode, the frequency parameter traces climb up and then decline, and may reach its crest around ϑ = 75°. Figure 4.7b shows that the 1st and 2nd mode frequency parameters of the plate have decreased slightly with the fiber direction angle ϑ increased (from 0 to 90°). And there is little variation in frequency parameters of the 3rd modes. Comparing with the lowest three modes, the 4th mode frequency curves in all subfigures have more significant changes which also climb up and then decline.

The effects of the fiber direction angle on frequency parameters and mode shapes of single-layered composite rectangular plates are further reported. In Tables 4.7 and 4.8, the lowest three frequency parameters Ω of a single-layered composite rectangular plate with various boundary conditions and fiber directions are presented. The aspect ratio is chosen to be b/a = 2/3. The thickness-to-width ratio h/b = 0.1 is used in the calculation. The fiber direction angle ϑ is varied from 0° to 90° with an increment of 15°. It can be noticed that increasing ϑ from 0° to 90°

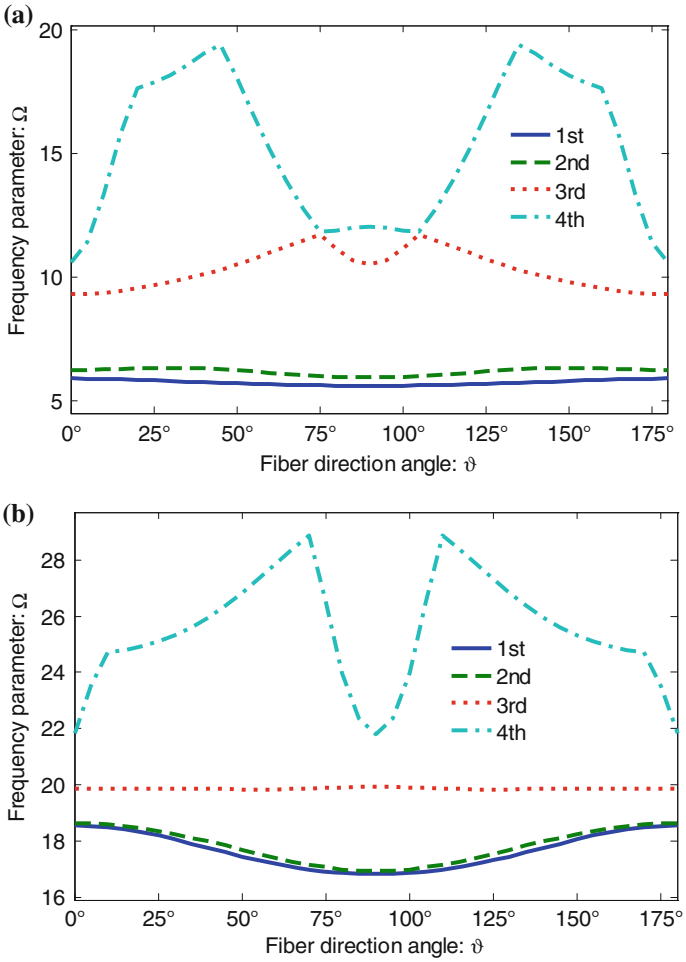

Fig. 4.7 Variation of the frequency parameters Ω versus the fiber direction angle ϑ for a [0°/ϑ/0°] laminated plate with different boundary conditions: **a** CFFF; **b** CFCF

increases the fundamental frequency parameters for plates with FSDSDSD, FCCC and FFFC boundary conditions. For the plates with orthotropy ratio $E_1/E_2 = 25$ and FFSDSD or FFFSD boundary conditions, when ϑ is varied from 0° to 45°, the fundamental frequency parameters increased as well. However, increasing the fiber direction angles from 45° to 90° decreases these frequency parameters. Furthermore, it can be seen from the table that the frequency parameters increase in general as the orthotropy ratio increases. Contour plots of the mode shapes for the plate with CCCC, FCCC and FFCC boundary conditions and orthotropy ratio $E_1/E_2 = 25$

Table 4.7 The first three frequency parameters Ω for a single-layered rectangular plate with various boundary conditions and fiber direction angles (b/a = 2/3, h/b = 0.1)

ϑ	Mode	E_1/E_2 = 5			E_1/E_2 = 25		
		FSDSDSD	FFSDSD	FFFSD	FSDSDSD	FFSDSD	FFFSD
0°	1	7.1214	1.8181	3.5800	7.1137	1.8435	3.5894
	2	15.243	10.782	9.8028	18.251	11.130	9.7959
	3	18.251	11.359	14.387	23.004	20.706	14.450
15°	1	7.4299	1.7988	3.8005	8.0005	1.9288	4.2139
	2	15.531	9.8858	10.017	20.939	10.880	10.023
	3	19.368	12.610	13.413	22.275	20.818	14.875
30°	1	8.2871	1.8809	4.1752	9.7757	2.1294	5.0365
	2	15.979	8.8869	10.716	21.598	9.8323	11.117
	3	21.867	14.214	12.576	27.293	20.197	15.100
45°	1	9.7045	1.9282	4.2298	12.792	2.2254	4.9192
	2	16.202	8.0423	10.768	21.975	8.6321	11.569
	3	23.053	16.088	13.950	30.772	18.577	18.381
60°	1	11.627	1.8796	3.9882	17.759	2.0992	4.3109
	2	16.507	7.4340	10.219	24.223	7.8529	10.792
	3	21.324	16.829	16.952	24.768	17.493	21.032
75°	1	13.407	1.7920	3.7406	20.110	1.8774	3.8508
	2	17.030	7.0324	9.7324	23.942	7.2353	9.9781
	3	19.144	16.453	19.485	26.949	16.736	20.346
90°	1	14.131	1.7831	3.6445	18.251	1.7886	3.6870
	2	17.333	6.9315	9.5416	27.073	6.9836	9.6477
	3	18.251	16.318	19.854	28.512	16.368	19.985

are given in Figs. 4.8, 4.9 and 4.10, respectively. From Figs. 4.8 and 4.10, we can see that the node lines (i.e., lines with zero displacements) of the second modes are paralleled to the fiber orientation.

Figure 4.11 shows the lowest three frequency parameters Ω and mode shapes for a FFFF, single-layered square composite plate with different fiber direction angles. The plate is assumed to be thin (h/a = 0.01) and made of material with orthotropy ratio E_1/E_2 = 25. Since the plate symmetrize about the line $x = y$, the frequency parameters for the plate with ϑ = 0°, 15° and 30° are the same as those with fiber direction angles ϑ = 90°, 75° and 60°, respectively. Similarly, mode shapes for ϑ = 0°, 15° and 30° are similar to those given for ϑ = 90°, 75° and 60°. In addition, it can be observed that the increment of the fiber direction angle from 0° to 45° results in increases of the lowest two frequency parameters of the plate.

Table 4.8 The first three frequency parameters Ω for a single-layered rectangular plate with various boundary conditions and fiber direction angles (b/a = 2/3, h/b = 0.1)

ϑ	Mode	E_1/E_2 = 5			E_1/E_2 = 25		
		FCCC	FFCC	FFFC	FCCC	FFCC	FFFC
0°	1	14.643	4.1554	2.2781	15.20202	5.9673	2.2701
	2	22.421	14.664	4.8398	30.26969	15.835	4.8543
	3	36.706	15.571	13.701	36.83315	25.755	13.704
15°	1	15.083	4.5393	2.3376	16.05186	6.9774	2.3549
	2	22.761	14.194	5.0506	30.07846	16.832	5.3525
	3	37.749	16.991	13.868	39.00083	26.250	14.089
30°	1	16.606	4.8977	2.5768	19.28065	7.5381	2.8620
	2	23.696	13.336	5.5623	30.81169	17.481	6.6963
	3	37.543	19.019	13.278	45.52704	27.112	15.349
45°	1	19.407	5.2668	3.0716	25.0631	8.4171	3.9445
	2	25.138	12.410	6.0661	33.3452	16.559	8.3679
	3	36.231	21.782	12.658	44.98416	28.239	15.340
60°	1	23.010	5.6496	3.7998	31.95584	9.6762	5.5627
	2	27.055	11.613	6.3853	37.2734	15.532	9.7606
	3	35.664	22.128	12.250	44.64113	25.914	15.519
75°	1	26.273	5.8850	4.6070	38.42538	10.791	8.0540
	2	28.954	10.957	6.5741	40.75042	14.863	10.835
	3	35.693	20.858	11.783	45.28074	23.461	15.109
90°	1	27.580	5.6969	5.0260	41.36358	10.730	10.436
	2	29.797	10.453	6.6394	42.27473	13.663	11.169
	3	35.804	20.259	11.530	45.79356	21.932	14.438

4.3.3 *Laminated Rectangular Plates with Elastic Boundary Conditions*

In order to prove the validity of the present method for the free vibration analysis of laminated plates with elastic boundary conditions, Table 4.9 shows the comparison of the first five frequency parameters $\Omega = \omega b^2/\pi^2\sqrt{\rho h/D}$ for $[0°/90°/0°\ldots]_9$ laminated plates with edges elastically restrained against rotation and translation (i.e. at edges $x = 0$ and a: $N_x = 0$, $N_{xy} = 0$, $k_w = \Gamma^* D_{22}/b^3$, $K_x = \Gamma^* D_{22}/b$, $M_{xy} = 0$ and at edges $y = 0$ and b: $N_{xy} = 0$, $N_y = 0$, $k_w = \Gamma^* D_{22}/a^3$, $M_{xy} = 0$, $K_y = \Gamma^* D_{22}/a$). The material constants and geometry parameters of the considered plates are: a/b = 1, E_1/E_2 = 40. The theoretical results reported by Liew et al. (1997) by using Pb2-Ritz method and Karami et al. (2006) based on DQM are included in the table. The results for thin (h/a = 0.001) and moderately thick plates (h/a = 0.2) with two different values of stiffness of elastic edges are found and are shown in the comparison. It is obvious that the proposed modified Fourier solution is sufficient to yield the solutions in good agreements with those of Pb2-Ritz method and DQM.

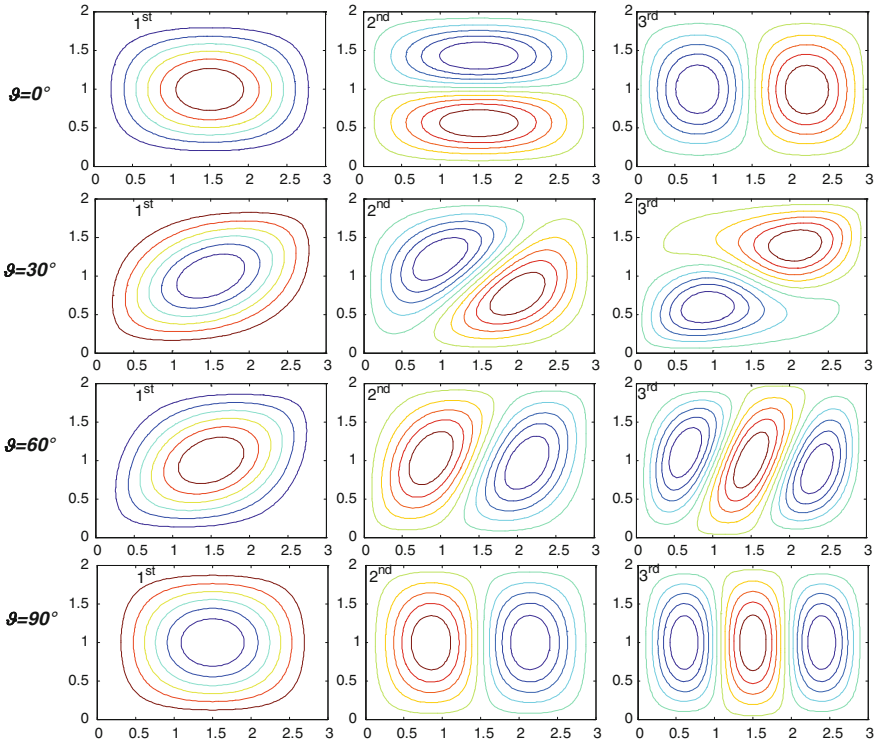

Fig. 4.8 Mode shapes for CCCC, single-layered rectangular plates (b/a = 2/3, h/b = 0.1, E_1/E_2 = 25)

In the last example in this section, vibration frequencies of composite laminated plates with some types of elastic restraints will be presented. Although we can obtain accurate solutions for composite laminated plates with arbitrary uniform and un-uniform elastic restraints, in this work, we choose three typical uniform elastic restraint conditions that are defined as follows (at $x = 0$):

E^1: the normal direction is elastically restrained ($u \neq 0$, $N_{xy} = Q_x = M_x = M_{xy} = 0$).
E^2: the transverse direction is elastically restrained ($w \neq 0$, $N_x = N_{xy} = M_x = M_{xy} = 0$).
E^3: the rotation is elastically restrained ($\phi_x \neq 0$, $N_x = N_{xy} = Q_x = M_{xy} = 0$).

Table 4.10 shows the lowest three frequency parameters Ω of laminated plates (E_1/E_2 = 20, a/b = 3/2) with different lamination schemes and thickness ratios. Two different lamination schemes, i.e. [0°/90°] and [0°/90°/0°], corresponding to symmetrically and unsymmetrically laminated plates are performed in the calculation. The thickness ratios used are h/a = 0.01, 0.05 and 0.1. The plates under consideration are clamped at the edge of $y = b$, free at edges $y = 0$, $x = a$ and with E^1 boundary conditions at the edge of $x = 0$ (E^1FFC). The table shows that increasing

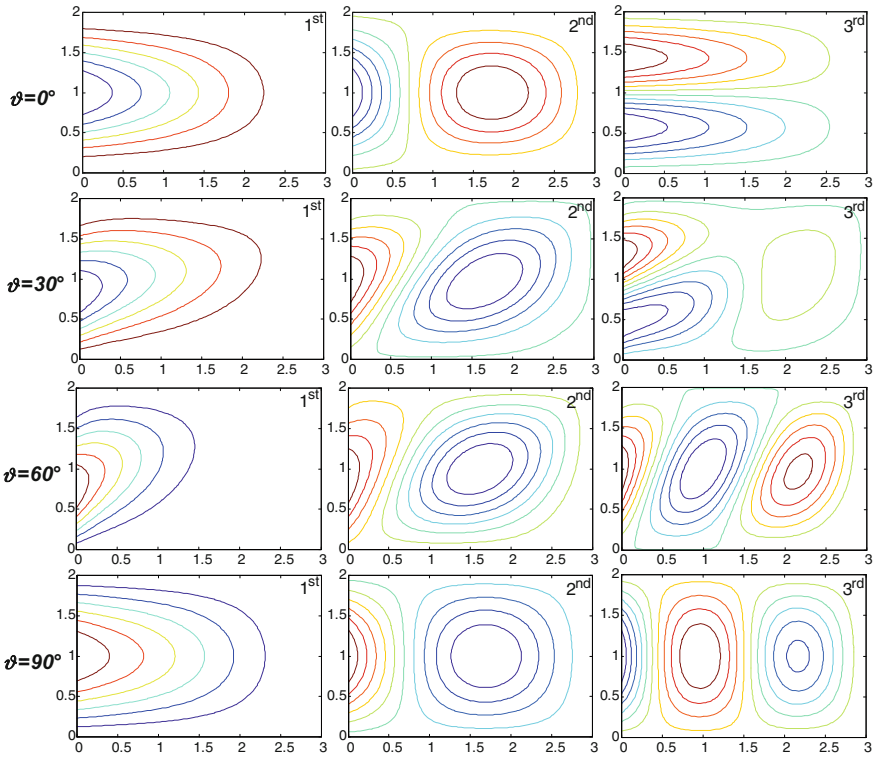

Fig. 4.9 Mode shapes for FCCC, single-layered rectangular plates (b/a = 2/3, h/b = 0.1, E_1/E_2 = 25)

the normal restrained rigidity has very limited effects on the frequency parameters of both symmetrically and unsymmetrically laminated plates. When the normal restrained rigidity is varied from $10^{-1}*D$ to $10^{4}*D$, the maximum increment in the table are less than 1.83 % for all cases. It may be attributed to the lower frequency parameters of a laminated plate with lower thickness ratios are dominated by the transverse vibration. The further observation from the table is that the effects for the [0°/90°] plate are larger than the [0°/90°/0°] one.

Tables 4.11 and 4.12 show similar studies for the E^2FFC and E^3FFC boundary conditions, respectively. Table 4.11 reveals that the transverse restrained rigidity has a large effect on the frequency parameters of both [0°/90°] and [0°/90°/0°] laminated plates, especially the second mode. When the transverse restrained rigidity is varied from $10^{-1}*D$ to $10^{4}*D$, the increments of the second mode can be 292.62, 286.48 and 263.75 % for the [0°/90°/0°] plate with thickness ratios of 0.01, 0.05 and 0.1, respectively. Table 4.12 shows that the rotation restrained rigidity has very limited effects on the fundamental frequency parameters of the plates, with the maximum increment less than 0.02 % in all cases when the rotation restrained rigidity is varied from $10^{-1}*D$ to $10^{4}*D$. However, for the second mode, increasing

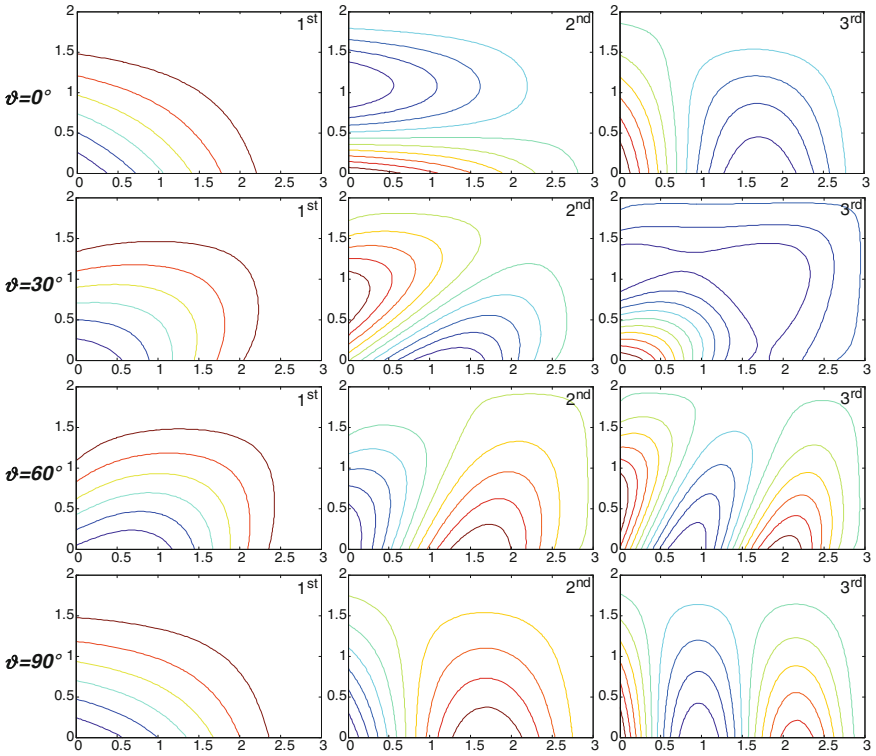

Fig. 4.10 Mode shapes for FFCC, single-layered rectangular plates (b/a = 2/3, h/b = 0.1, E_1/E_2 = 25)

the rotation restrained rigidity from $10^{-1}*D$ to $10^{4}*D$ increases the frequency parameters by almost 8 and 50 % in each plate configuration. From these tables, it is obvious that the effects of elastic restraint rigidity on the frequency parameters of composite laminated plates varies with mode sequences, lamination schemes and spring components. These results may serve as benchmark solutions for further researchers.

4.3.4 Laminated Rectangular Plates with Internal Line Supports

In the engineering practices, laminated plates are often restrained by internal line supports to reduce the magnitude of dynamic and static stresses and displacements of the structure or satisfy special architectural and functional requirements. The study of the vibrations of laminated plates with internal line supports is an important aspect in the successful applications of these structures. Thus, in this part,

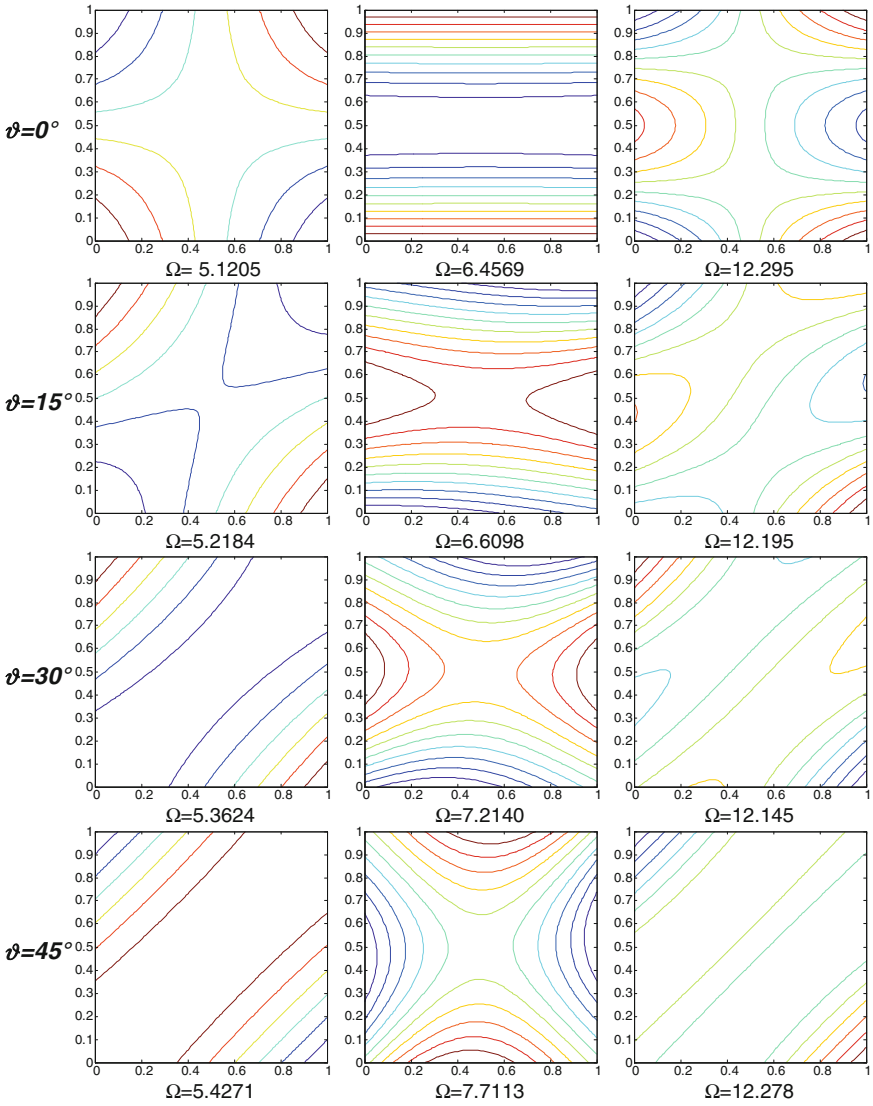

Fig. 4.11 Frequency parameters Ω and mode shapes for FFFF, thin single-layered square plates (h/a = 0.01, E_1/E_2 = 25)

the present method is applied to investigate the free vibration behaviors of laminated rectangular plates with internal line supports and arbitrary boundary conditions. As shown in Fig. 4.12, a laminated rectangular plate restrained by arbitrary internal line supports is considered. x_i and y_j represent the position of the ith and jth line supports along the y- and x-axes, respectively. The displacement fields in the position of the line support satisfy $w\ (x_i,\ y) = 0$ and $w\ (x,\ y_j) = 0$ (Cheung and Zhou

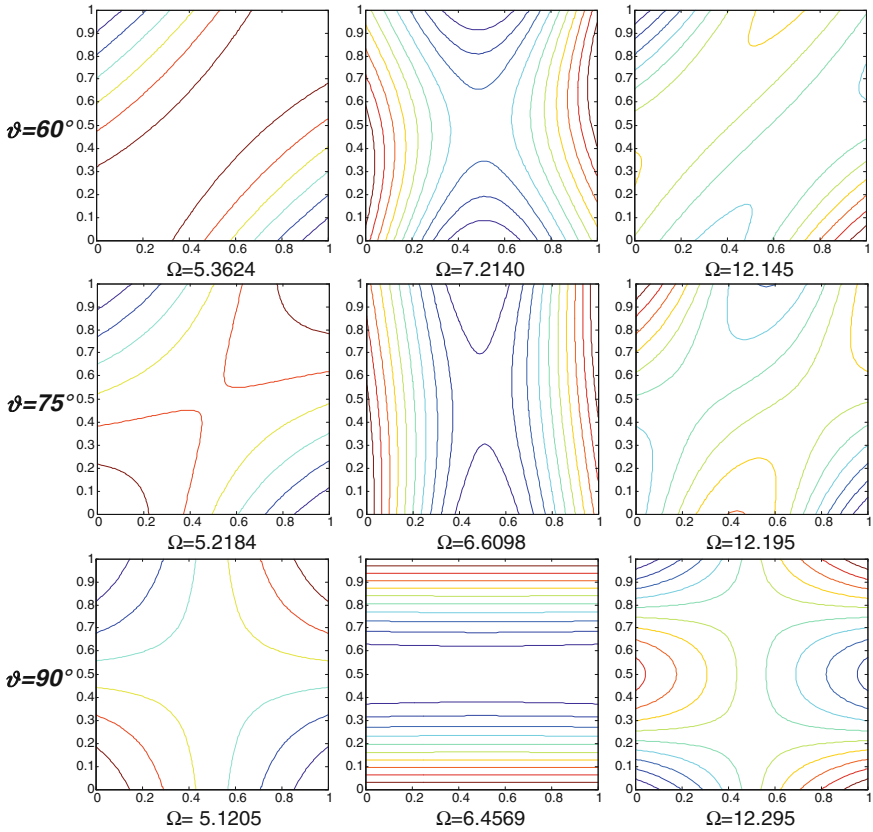

Fig. 4.11 (continued)

2001a, b). This condition can be readily obtained by introducing a group of continuously distributed linear springs at the location of each line support and setting the stiffness of these springs equal to infinite (which is represented by a very large number, $10^7 * D$). Thus, the potential energy (P_{ils}) stored in these springs is:

$$P_{ils} = \frac{1}{2}\int_0^b \left\{\sum_{i=1}^{N_i} k_{xi}^i w(x_i, y)^2\right\} dy + \frac{1}{2}\int_0^a \left\{\sum_{j=1}^{M_j} k_{yj}^j w(x, y_j)^2\right\} dx \tag{4.34}$$

where N_i and M_j are the amount of line supports in the y and x directions. k_{xi}^i, k_{yj}^j denote the corresponding line supported springs distributed at $x = x_i$ and $y = y_j$. By adding the potential energy P_{ils} functions in the Lagrangian energy functional and applying the weak form solution procedure, the characteristic equation for a plate with arbitrary boundary conditions and internal line supports is readily obtained.

Table 4.9 Comparison of the frequency parameters $\Omega = \omega b^2/\pi^2\sqrt{\rho h/D}$ for a $[0°/90°/0°\ldots]_9$ laminated plate with edges elastically restrained against rotation and translation (a/b = 1, E_1/E_2 = 40)

Γ	h/a	Method	Mode number				
			1	2	3	4	5
10^2	0.001	Present	1.8096	2.5703	2.7234	3.3061	4.6721
		Karami et al. (2006)	1.8095	2.5703	2.7234	3.3061	4.6721
		Liew et al. (1997)	1.8096	2.5703	2.7234	3.3061	4.6721
	0.2	Present	1.1236	1.7134	1.7635	2.1909	2.5323
		Karami et al. (2006)	1.1236	1.7134	1.7636	2.1909	2.5323
		Liew et al. (1997)	1.1236	1.7134	1.7636	2.1909	2.5323
10^8	0.001	Present	3.9126	7.0767	9.0087	10.878	12.743
		Karami et al. (2006)	3.9126	7.0767	9.0087	10.878	12.743
		Liew et al. (1997)	3.9126	7.0743	9.0088	10.878	12.744
	0.2	Present	1.3177	2.0543	2.1064	2.6346	2.9945
		Karami et al. (2006)	1.3177	2.0543	2.1064	2.6346	2.9946
		Liew et al. (1997)	1.3177	2.0543	2.1064	2.6346	2.9945

Table 4.10 The first three frequency parameters Ω for laminated rectangular plates with E^1FFC boundary conditions and different thickness ratios (E_1/E_2 = 20, a/b = 3/2)

h/a	k_{x0}^u/D	[0°/90°]			[0°/90°/0°]		
		1	2	3	1	2	3
0.01	10^{-1}	4.6013	6.5918	16.506	2.9838	5.5004	18.670
	10^0	4.6013	6.5920	16.507	2.9838	5.5004	18.670
	10^1	4.6013	6.5939	16.512	2.9838	5.5004	18.670
	10^2	4.6013	6.6070	16.554	2.9838	5.5004	18.670
	10^3	4.6014	6.6536	16.707	2.9838	5.5004	18.670
	10^4	4.6014	6.6846	16.809	2.9838	5.5004	18.670
0.05	10^{-1}	4.5518	6.4066	15.935	2.9686	5.3613	18.045
	10^0	4.5518	6.4124	15.954	2.9686	5.3613	18.047
	10^1	4.5518	6.4356	16.012	2.9686	5.3613	18.045
	10^2	4.5518	6.4874	16.165	2.9686	5.3613	18.048
	10^3	4.5518	6.5046	16.197	2.9686	5.3613	18.048
	10^4	4.5518	6.5158	16.205	2.9686	5.3613	18.044
0.10	10^{-1}	4.4076	6.0284	14.736	2.9232	5.1045	16.449
	10^0	4.4076	6.0435	14.795	2.9232	5.1045	16.449
	10^1	4.4076	6.0917	14.812	2.9232	5.1045	16.449
	10^2	4.4076	6.1232	14.693	2.9232	5.1045	16.449
	10^3	4.4076	6.1250	14.827	2.9232	5.1045	16.449
	10^4	4.4076	6.1250	14.825	2.9232	5.1045	16.449

Table 4.11 The first three frequency parameters Ω for laminated rectangular plates with E^2FFC boundary conditions and different thickness ratios (E_1/E_2 = 20, a/b = 3/2)

h/a	k_{x0}^w/D	[0°/90°]			[0°/90°/0°]		
		1	2	3	1	2	3
0.01	10^{-1}	4.8727	7.5360	17.057	3.3908	6.7176	18.785
	10^{0}	5.1045	10.714	21.873	3.7219	12.806	19.279
	10^{1}	5.1603	12.039	29.342	3.8062	19.314	19.938
	10^{2}	5.1724	12.198	29.386	3.8233	19.632	20.806
	10^{3}	5.1751	12.217	29.393	3.8268	19.652	20.911
	10^{4}	5.1760	12.221	29.395	3.8280	19.657	20.922
0.05	10^{-1}	4.8173	7.3853	16.448	3.3651	6.5993	18.162
	10^{0}	5.0194	10.468	21.285	3.6688	12.578	18.618
	10^{1}	5.0688	11.701	27.306	3.7430	18.529	19.135
	10^{2}	5.0781	11.841	27.343	3.7574	18.869	19.801
	10^{3}	5.0848	11.816	27.346	3.7626	18.893	19.889
	10^{4}	5.0820	11.846	27.353	3.7635	18.906	19.893
0.10	10^{-1}	4.6552	7.0274	15.301	3.3015	6.3737	16.568
	10^{0}	4.8229	9.9146	17.015	3.5636	11.976	16.810
	10^{1}	4.8608	10.922	17.018	3.6276	16.595	16.808
	10^{2}	4.8681	11.037	17.018	3.6370	16.810	17.028
	10^{3}	4.8690	11.051	17.013	3.6387	16.809	17.054
	10^{4}	4.8695	11.045	17.019	3.6354	16.810	17.051

In order to prove the validity of the present method in dealing with vibration of laminated composite plate with internal line supports, Table 4.13 presents the comparison of the first nine frequency parameters $\Omega = \omega ab\sqrt{\rho h/D}$ for a square cross-ply [0°/90°] laminated plate with a central line support in each direction. The material used is graphite-epoxy with the following proprieties: E_1/E_2 = 40, $\mu_{12} = 0.25$, $G_{12} = 0.5E_2$, $G_{13} = 0.5E_2$, $G_{23} = 0.2E_2$. Three different classical boundary conditions, i.e. FFFF, SDSDSDSD and CCCC are considered in the comparison. The benchmark solutions provided by Cheung and Zhou (2001a) based on CPT are referenced. From the table a consistent agreement of present results and referential date is seen. The discrepancy is very small and does not exceeds 0.52 % for the worst case although different trial functions are used in the literature. In addition, the table shows that the line supports increase the frequencies of the plate.

Influence of the locations of line supports on the frequency parameters of a three-layered, cross-ply [0°/90°/0°] plate is investigated as well. The plate is assumed to be thick (h/b = 0.2) and with similar material parameters as those used in Table 4.13. For the sake of brevity, only a line support along y direction (x_1) is considered in the analysis. In Fig. 4.13, variations of the lowest three mode frequency parameters $\Omega = \omega ab\sqrt{\rho h/D}$ of the considered plate with high length–width ratio (a/b = 5)

Table 4.12 The first three frequency parameters Ω for laminated rectangular plates with E^3FFC boundary conditions and different thickness ratios (E_1/E_2 = 20, a/b = 3/2)

h/a	K_{x0}^{x}/D	[0°/90°]			[0°/90°/0°]		
		1	2	3	1	2	3
0.01	10^{-1}	4.6014	6.8477	17.434	2.9838	5.9550	18.671
	10^{0}	4.6014	7.2371	19.370	2.9840	7.5831	18.675
	10^{1}	4.6014	7.3529	20.096	2.9842	8.7787	18.678
	10^{2}	4.6014	7.3669	20.188	2.9843	8.9800	18.679
	10^{3}	4.6014	7.3682	20.197	2.9843	9.0014	18.679
	10^{4}	4.6014	7.3684	20.198	2.9843	9.0037	18.679
0.05	10^{-1}	4.5518	6.6726	16.843	2.9687	5.8207	18.047
	10^{0}	4.5518	7.0598	18.688	2.9690	7.4238	18.048
	10^{1}	4.5518	7.1817	19.364	2.9691	8.5934	18.054
	10^{2}	4.5518	7.1886	19.444	2.9692	8.7857	18.055
	10^{3}	4.5518	7.1878	19.495	2.9692	8.8088	18.056
	10^{4}	4.5518	7.2143	19.457	2.9692	8.8104	18.054
0.10	10^{-1}	4.4076	6.3041	15.549	2.9233	5.5674	16.450
	10^{0}	4.4077	6.6868	17.012	2.9235	7.1204	16.453
	10^{1}	4.4078	6.7927	17.019	2.9238	8.1643	16.455
	10^{2}	4.4078	6.8034	17.018	2.9238	8.3348	16.456
	10^{3}	4.4078	6.8054	17.018	2.9239	8.3503	16.456
	10^{4}	4.4078	6.8064	17.018	2.9239	8.3667	16.456

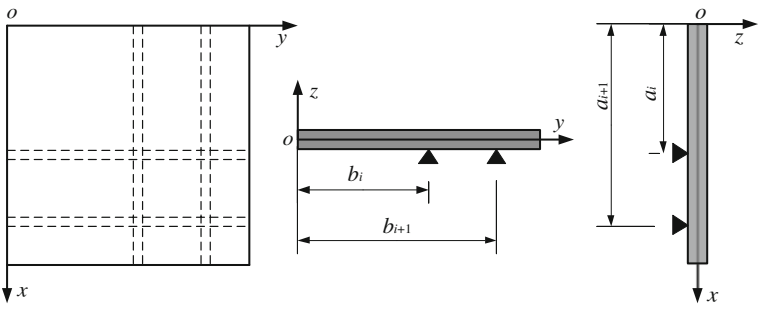

Fig. 4.12 Schematic diagram of laminated rectangular plates with arbitrary internal line supports

against the line support location parameter x_1/a are depicted. Six types of edge conditions used in the investigation are: F–S, S–F, S–S, C–C, F–C and C–F. It is obvious that the frequency parameters of the plate are significantly affected by the position of the line support, and this effect can vary with the boundary conditions. And for different modes, the effects of line support location are quite different. For the sake of completeness, the similar studies for the considered plate with lower

Table 4.13 Comparison of the first five frequency parameters $\Omega = \omega ab\sqrt{\rho h/D}$ for a square, [0°/90°] laminated plate with a central line support in each direction (h/a = 0.001)

Boundary conditions	Method	Mode number				
		1	2	3	4	5
FFFF	Present	2.636	6.569	6.569	9.005	26.046
	Cheung and Zhou (2001a)	2.631	6.572	6.572	9.006	26.067
	Error (%)	0.19	0.05	0.05	0.01	0.08
SDSDSDSD	Present	24.438	31.348	31.383	37.078	68.539
SDSDSDSD	Cheung and Zhou (2001a)	24.440	31.333	31.333	36.989	68.549
	Error (%)	0.01	0.05	0.16	0.24	0.01
CCCC	Present	36.971	45.505	45.563	52.703	87.040
	Cheung and Zhou (2001a)	37.002	45.528	45.528	52.695	87.499
	Error (%)	0.08	0.05	0.08	0.02	0.52

length-width ratio (a/b = 1) are presented in Fig. 4.14. Comparing Figs. 4.13 with 4.14, we can see that the influence of the line support location on the frequency parameters vary with length-width ratios and boundary conditions.

4.4 Fundamental Equations of Laminated Sectorial, Annular and Circular Plates

The sectorial, annular and circular plates are plates of circular peripheries. They are used quite often in aerospace crafts, naval vessels, civil constructions and other fields of modern technology. When dealing with these plates, it is expedient to use polar coordinate system in the formulation. Sectorial, annular and circular plates made of isotropic materials have received considerable attention in the literature. When compared with the amount of information available for isotropic sectorial, annular and circular plates, studies reported on the vibration analysis of orthotropic and laminated sectorial, annular and circular plates are very limited. This can be due to the difficulty in constructing such plates. There commonly exist two types of orthotropic sectorial, annular and circular plates. The first type is to actually construct the plates with rectangular orthotropy and then cut the plates in sectorial, annular or circular shapes. On the other hand, one can also construct circular plates that the material principle directions take a circular shape around the center of the plates, thus results in polar orthotropy, and then cut the plates in sectorial, annular or circular shapes with desired geometry dimensions. The section deals with vibration of laminated sectorial, annular and circular plates made of layers having

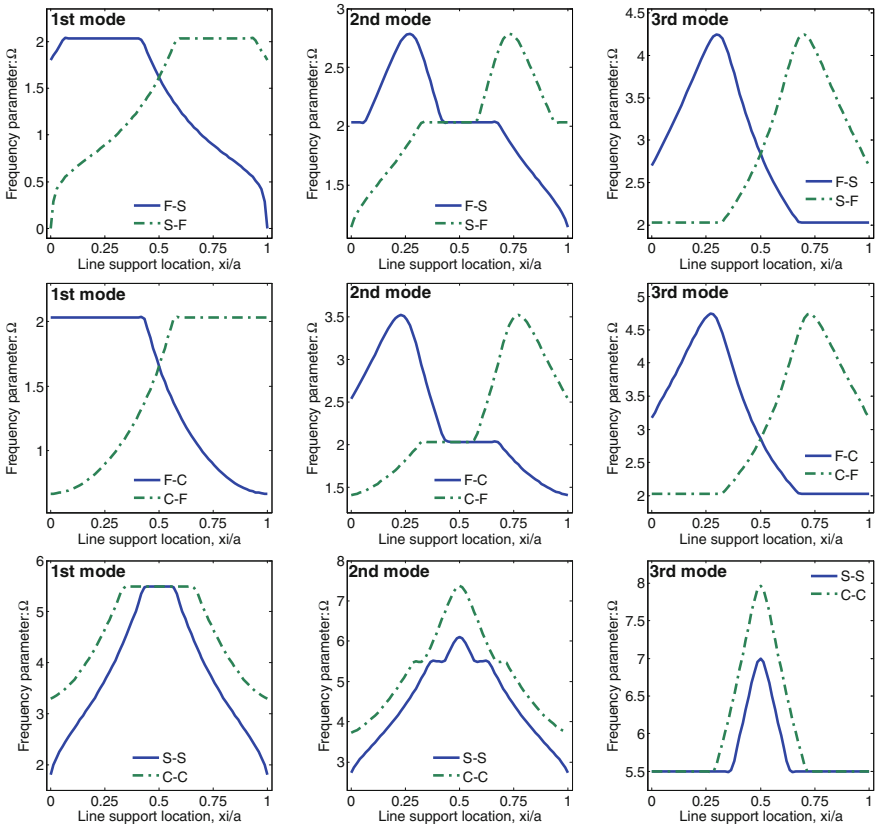

Fig. 4.13 Variation of the frequency parameters $\Omega = \omega ab\sqrt{\rho h/D}$ versus the line support locations for a long (a/b = 5), [0°/90°/0°] laminated plate with a y direction internal line support

polar orthotropy (i.e., lamination angle of 0° or 90°). The corresponding isotropic ones are considered as well.

Annular and circular plates can be treated as special cases of sectorial plates with circumferential direction of full circle (2π). As shown in Fig. 4.15, a general laminated sectorial plate of circumferential direction θ_0, constant thickness h, inner radius R_0 and outer radius R_1 is selected as the analysis model. Polar coordinate system (r, θ and z) located at the middle surface of the plate is used for plate coordinates, in which z is parallel to the thickness direction. The middle surface displacements of the plate in the r, θ and z directions are denoted by u, v and w, respectively. The laminated sectorial plate is assumed to be composed of N_L layers of polar orthotropic laminae.

Consider the sectorial plate in Fig. 4.15 and its polar coordinate system. The following geometry parameters can be applied to the shell equations derived in Chap. 1 to obtain those of sectorial, annular and circular plates.

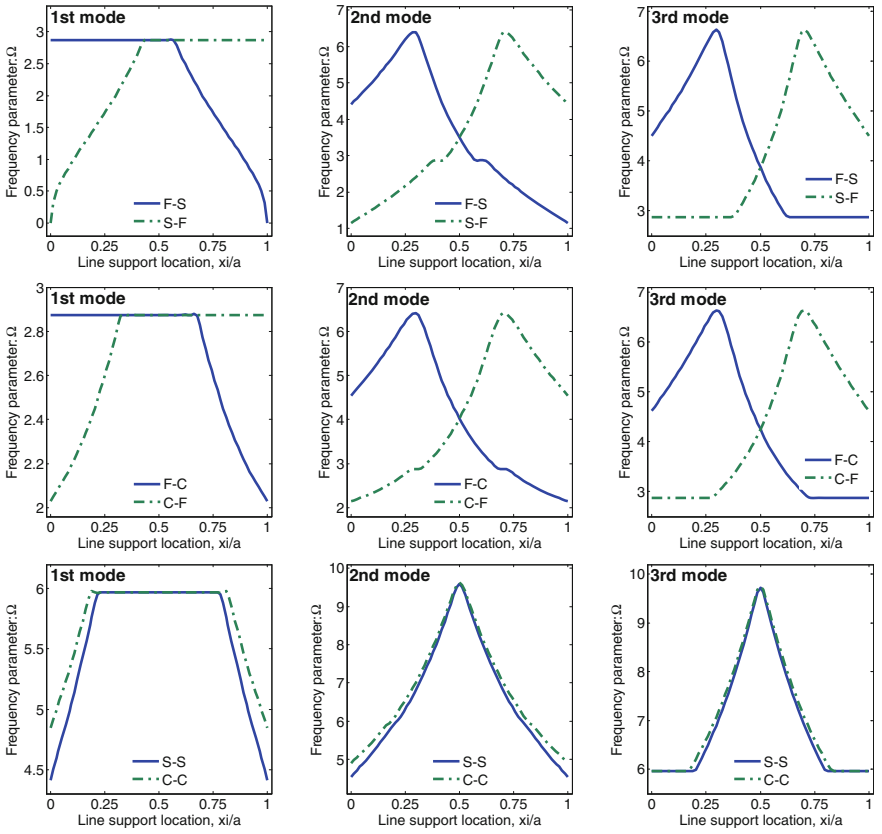

Fig. 4.14 Variation of the frequency parameters $\Omega = \omega ab\sqrt{\rho h/D}$ versus the line support locations for a square, [0°/90°/0°] laminated plate with a y direction internal line support

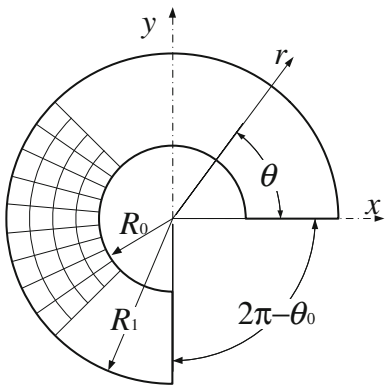

Fig. 4.15 Geometry and coordinate system of laminated sectorial plates with polar orthotropy

$$\alpha = r, \quad \beta = \theta, \quad A = 1, \quad B = r, \quad R_\alpha = \infty, \quad R_\beta = \infty \tag{4.35}$$

We will first derive the fundamental equations for the thin plates (neglecting shear deformation and rotary inertia), followed by the thick ones. For the sake of brevity, the annular and circular plates will be treated as the special cases of sectorial plates in the following formulation.

4.4.1 Fundamental Equations of Thin Laminated Sectorial, Annular and Circular Plates

Substituting Eq. (4.35) into Eq. (1.7), the middle surface strains, curvature and twist changes of a sectorial plate can be written as:

$$\begin{aligned} \varepsilon_r^0 &= \frac{\partial u}{\partial r}, & \chi_r &= -\frac{\partial^2 w}{\partial r^2} \\ \varepsilon_\theta^0 &= \frac{\partial v}{r\partial\theta} + \frac{u}{r}, & \chi_\theta &= -\frac{\partial^2 w}{r^2\partial\theta^2} - \frac{\partial w}{r\partial r} \\ \gamma_{r\theta}^0 &= \frac{\partial v}{\partial r} + \frac{\partial u}{r\partial\theta} - \frac{v}{r}, & \chi_{r\theta} &= -2\frac{\partial^2 w}{r\partial r\partial\theta} + \frac{\partial w}{2r^2\partial\theta} \end{aligned} \tag{4.36}$$

Thus, the strain-displacement relations for an arbitrary point in the plate space can be defined as:

$$\begin{aligned} \varepsilon_r &= \varepsilon_r^0 + z\chi_r \\ \varepsilon_\theta &= \varepsilon_\theta^0 + z\chi_\theta \\ \gamma_{r\theta} &= \gamma_{r\theta}^0 + z\chi_{r\theta} \end{aligned} \tag{4.37}$$

Considering Hooke's law, the corresponding stresses in the plate space are:

$$\begin{Bmatrix} \sigma_r \\ \sigma_\theta \\ \tau_{r\theta} \end{Bmatrix}_k = \begin{bmatrix} \overline{Q_{11}^k} & \overline{Q_{12}^k} & \overline{Q_{16}^k} \\ \overline{Q_{12}^k} & \overline{Q_{22}^k} & \overline{Q_{26}^k} \\ \overline{Q_{16}^k} & \overline{Q_{26}^k} & \overline{Q_{66}^k} \end{bmatrix} \begin{Bmatrix} \varepsilon_r \\ \varepsilon_\theta \\ \gamma_{r\theta} \end{Bmatrix}_k \tag{4.38}$$

The lamina stiffness coefficients $\overline{Q_{ij}^k}$ (i, j = 1, 2, 6) are given in Eq. (1.12). By carrying the integration of stresses over the cross-section, the force and moment resultants can be obtained in terms of the middle surface strains and curvature changes as

$$\begin{bmatrix} N_r \\ N_\theta \\ N_{r\theta} \\ M_r \\ M_\theta \\ M_{r\theta} \end{bmatrix} = \begin{bmatrix} A_{11} & A_{12} & A_{16} & B_{11} & B_{12} & B_{16} \\ A_{12} & A_{22} & A_{26} & B_{12} & B_{22} & B_{26} \\ A_{16} & A_{26} & A_{66} & B_{16} & B_{26} & B_{66} \\ B_{11} & B_{12} & B_{16} & D_{11} & D_{12} & D_{16} \\ B_{12} & B_{22} & B_{26} & D_{12} & D_{22} & D_{26} \\ B_{16} & B_{26} & B_{66} & D_{16} & D_{26} & D_{66} \end{bmatrix} \begin{bmatrix} \varepsilon_r^0 \\ \varepsilon_\theta^0 \\ \gamma_{r\theta}^0 \\ \chi_r \\ \chi_\theta \\ \chi_{r\theta} \end{bmatrix} \tag{4.39}$$

where N_r, N_θ and $N_{r\theta}$ are the normal and shear force resultants and M_r, M_θ, $M_{r\theta}$ denote the bending and twisting moment resultants. A_{ij}, B_{ij}, and D_{ij} are the stiffness coefficients arising from the piecewise integration over the plate thickness direction, they can be written as in Eq. (1.15).

Substituting Eq. (4.35) into Eqs. (1.16), (1.17), (1.19) and (1.21), the energy functions of a sectorial plate with general boundary conditions can be obtained.

$$U_s = \frac{1}{2}\int_r \int_\theta \left\{ \begin{matrix} N_r\varepsilon_r^0 + N_\theta\varepsilon_\theta^0 + N_{r\theta}\gamma_{r\theta}^0 \\ +M_r\chi_r + M_\theta\chi_\theta + M_{r\theta}\chi_{r\theta} \end{matrix} \right\} r dr d\theta \tag{4.40a}$$

$$T = \frac{1}{2}\int_r \int_\theta I_0 \left\{ (\partial u/\partial t)^2 + (\partial v/\partial t)^2 + (\partial w/\partial t)^2 \right\} r dr d\theta \tag{4.40b}$$

$$W_e = \int_r \int_\theta \{q_r u + q_\theta v + q_z w\} r dr d\theta \tag{4.40c}$$

$$\begin{aligned} U_{sp} = & \frac{1}{2}\int_\theta \left\{ \begin{matrix} \left[k_{r0}^u u^2 + k_{r0}^v v^2 + k_{r0}^w w^2 + K_{r0}^w (\partial w/\partial r)^2 \right]_{r=R_0} \\ + \left[k_{r1}^u u^2 + k_{r1}^v v^2 + k_{r1}^w w^2 + K_{r1}^w (\partial w/\partial r)^2 \right]_{r=R_1} \end{matrix} \right\} r d\theta \\ & + \frac{1}{2}\int_r \left\{ \begin{matrix} \left[k_{\theta 0}^u u^2 + k_{\theta 0}^v v^2 + k_{\theta 0}^w w^2 + K_{\theta 0}^w (\partial w/r\partial\theta)^2 \right]_{\theta=0} \\ + \left[k_{\theta 1}^u u^2 + k_{\theta 1}^v v^2 + k_{\theta 1}^w w^2 + K_{\theta 1}^w (\partial w/r\partial\theta)^2 \right]_{\theta=\theta_0} \end{matrix} \right\} dr \end{aligned} \tag{4.40d}$$

where U_s and T are the stain and kinetic energy functions. W_e represents external work done by the external loads, in which q_r, q_θ and q_z denote the external loads in the r, θ and z directions, respectively. U_{sp} is boundary spring deformation energy function introduced by the artificial spring boundary technique (see Sect. 1.2.3 and Fig. 4.16).

Specializing Eqs. (1.33) and (1.34) to those of sectorial plates results in following governing equations

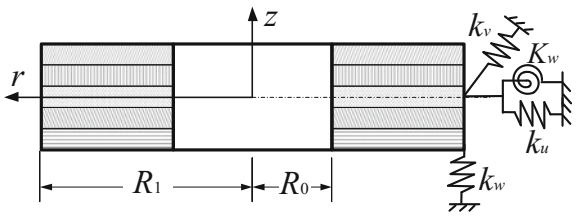

Fig. 4.16 Boundary conditions of a thin laminated sectorial plate

$$\begin{aligned}
&\frac{\partial(rN_r)}{\partial r}+\frac{\partial(N_{r\theta})}{\partial\theta}-N_\theta+rq_r=rI_0\frac{\partial^2 u}{\partial t^2}\\
&\frac{\partial(rN_{r\theta})}{\partial r}+\frac{\partial(N_\theta)}{\partial\theta}+N_{r\theta}+rq_\theta=rI_0\frac{\partial^2 v}{\partial t^2}\\
&\frac{\partial(rQ_r)}{\partial r}+\frac{\partial(Q_\theta)}{\partial\theta}+rq_z=rI_0\frac{\partial^2 w}{\partial t^2}
\end{aligned}\tag{4.41}$$

where

$$\begin{aligned}
Q_r&=\frac{\partial(rM_r)}{r\partial r}+\frac{\partial(M_{r\theta})}{r\partial\theta}-\frac{M_\theta}{r}\\
Q_\theta&=\frac{\partial(M_\theta)}{r\partial\theta}+\frac{\partial(rM_{r\theta})}{r\partial r}+\frac{M_{r\theta}}{r}
\end{aligned}\tag{4.42}$$

For a sectorial plate symmetrically laminated with respect to the middle surface, the first two governing equations are decoupled from the third one, i.e., the in-plane vibration (u, v) will be decoupled from the bending vibration (w). The corresponding boundary conditions of thin laminated sectorial plates are:

$$r=R_0:\begin{cases}N_r-k_{r0}^u u=0\\ N_{r\theta}-k_{r0}^v v=0\\ Q_r+\dfrac{\partial M_{r\theta}}{r\partial\theta}-k_{r0}^w w=0\\ -M_r-K_{r0}^w\dfrac{\partial w}{\partial r}=0\end{cases}\qquad r=R_1:\begin{cases}N_r+k_{r1}^u u=0\\ N_{r\theta}+k_{r1}^v v=0\\ Q_r+\dfrac{\partial M_{r\theta}}{r\partial\theta}+k_{r1}^w w=0\\ -M_r+K_{r1}^w\dfrac{\partial w}{\partial r}=0\end{cases}$$

$$\theta=0:\begin{cases}N_{r\theta}-k_{\theta0}^u u=0\\ N_\theta-k_{\theta0}^v v=0\\ Q_\theta+\dfrac{\partial M_{r\theta}}{\partial r}-k_{\theta0}^w w=0\\ -M_\theta-K_{\theta0}^w\dfrac{\partial w}{r\partial\theta}=0\end{cases}\qquad \theta=\theta_0:\begin{cases}N_{r\theta}+k_{\theta1}^u u=0\\ N_\theta+k_{\theta1}^v v=0\\ Q_\theta+\dfrac{\partial M_{r\theta}}{\partial r}+k_{\theta1}^w w=0\\ -M_\theta+K_{\theta1}^w\dfrac{\partial w}{r\partial\theta}=0\end{cases}\tag{4.43}$$

4.4.2 Fundamental Equations of Thick Laminated Sectorial, Annular and Circular Plates

Fundamental equations of thick sectorial plates are obtained by directly substituting Eq. (4.35) into those of thick laminated shells given in Sect. 1.3.

In the framework of first-order shear deformation plate theory, the displacement field in an arbitrary point of a thick laminated sectorial plate is expressed in terms of middle surface displacements and rotation components as:

$$\begin{aligned} U(r,\theta,z) &= u(r,\theta) + z\phi_r(r,\theta) \\ V(r,\theta,z) &= v(r,\theta) + z\phi_\theta(r,\theta) \\ W(r,\theta,z) &= w(r,\theta) \end{aligned} \tag{4.44}$$

where ϕ_r and ϕ_θ represent the rotations of transverse normal respect to θ and r directions. Thus, the corresponding strains at this point are defined in terms of middle surface strains, curvature and twist changes as

$$\begin{aligned} \varepsilon_r &= \varepsilon_r^0 + z\chi_r, & \gamma_{rz} &= \gamma_{rz}^0 \\ \varepsilon_\theta &= \varepsilon_\theta^0 + z\chi_\theta, & \gamma_{\theta z} &= \gamma_{\theta z}^0 \\ \gamma_{r\theta} &= \gamma_{r\theta}^0 + z\chi_{r\theta} \end{aligned} \tag{4.45}$$

where the middle surface strains and curvature and twist changes are written as:

$$\begin{aligned} \varepsilon_r^0 &= \frac{\partial u}{\partial r}, & \chi_r &= \frac{\partial \phi_r}{\partial r} \\ \varepsilon_\theta^0 &= \frac{\partial v}{r\partial\theta} + \frac{u}{r}, & \chi_\theta &= \frac{\partial \phi_\theta}{r\partial\theta} + \frac{\phi_r}{r} \\ \gamma_{r\theta}^0 &= \frac{\partial v}{\partial r} + \frac{\partial u}{r\partial\theta} - \frac{v}{r}, & \chi_{r\theta} &= \frac{\partial \phi_\theta}{\partial r} + \frac{\partial \phi_r}{r\partial\theta} - \frac{\phi_\theta}{r} \\ \gamma_{rz}^0 &= \frac{\partial w}{\partial r} + \phi_r \\ \gamma_{\theta z}^0 &= \frac{\partial w}{r\partial\theta} + \phi_\theta \end{aligned} \tag{4.46}$$

According to Eqs. (1.46) and (1.47), the force and moment resultant equations of thick sectorial plates become:

$$\begin{bmatrix} N_r \\ N_\theta \\ N_{r\theta} \\ M_r \\ M_\theta \\ M_{r\theta} \end{bmatrix} = \begin{bmatrix} A_{11} & A_{12} & A_{16} & B_{11} & B_{12} & B_{16} \\ A_{12} & A_{22} & A_{26} & B_{12} & B_{22} & B_{26} \\ A_{16} & A_{26} & A_{66} & B_{16} & B_{26} & B_{66} \\ B_{11} & B_{12} & B_{16} & D_{11} & D_{12} & D_{16} \\ B_{12} & B_{22} & B_{26} & D_{12} & D_{22} & D_{26} \\ B_{16} & B_{26} & B_{66} & D_{16} & D_{26} & D_{66} \end{bmatrix} \begin{bmatrix} \varepsilon_r^0 \\ \varepsilon_\theta^0 \\ \gamma_{r\theta}^0 \\ \chi_r \\ \chi_\theta \\ \chi_{r\theta} \end{bmatrix} \tag{4.47}$$

$$\begin{bmatrix} Q_\theta \\ Q_r \end{bmatrix} = \begin{bmatrix} A_{44} & A_{45} \\ A_{45} & A_{55} \end{bmatrix} \begin{bmatrix} \gamma^0_{\theta z} \\ \gamma^0_{rz} \end{bmatrix} \tag{4.48}$$

Substituting Eq. (4.35) into Eqs. (1.49), (1.51), (1.53) and (1.54) yields the energy functions of a sectorial plate including shear deformation and rotary inertia:

$$U_s = \frac{1}{2}\int_r \int_\theta \left\{ \begin{array}{l} N_r\varepsilon^0_r + N_\theta\varepsilon^0_\theta + N_{r\theta}\gamma^0_{r\theta} + M_r\chi_r \\ +M_\theta\chi_\theta + M_{r\theta}\chi_{r\theta} + Q_r\gamma^0_{rz} + Q_\theta\gamma^0_{\theta z} \end{array} \right\} r dr d\theta \tag{4.49a}$$

$$T = \frac{1}{2}\int_r \int_\theta \left\{ \begin{array}{l} I_0\left(\frac{\partial u}{\partial t}\right)^2 + I_0\left(\frac{\partial v}{\partial t}\right)^2 + I_0\left(\frac{\partial w}{\partial t}\right)^2 + I_2\left(\frac{\partial \phi_r}{\partial t}\right)^2 \\ +2I_1\frac{\partial u}{\partial t}\frac{\partial \phi_r}{\partial t} + 2I_1\frac{\partial v}{\partial t}\frac{\partial \phi_\theta}{\partial t} + I_2\left(\frac{\partial \phi_\theta}{\partial t}\right)^2 \end{array} \right\} r dr d\theta \tag{4.49b}$$

$$W_e = \int_r \int_\theta \{q_r u + q_\theta v + q_z w + m_r\phi_r + m_\theta\phi_\theta\} r dr d\theta \tag{4.49c}$$

$$\begin{aligned} U_{sp} = & \frac{1}{2}\int_\theta \left\{ \begin{array}{l} \left[k^u_{r0}u^2 + k^v_{r0}v^2 + k^w_{r0}w^2 + K^r_{r0}\phi^2_r + K^\theta_{r0}\phi^2_r\right]_{r=R_0} \\ +\left[k^u_{r1}u^2 + k^v_{r1}v^2 + k^w_{r1}w^2 + K^r_{r1}\phi^2_r + K^\theta_{r1}\phi^2_r\right]_{r=R_1} \end{array} \right\} r d\theta \\ & + \frac{1}{2}\int_r \left\{ \begin{array}{l} \left[k^u_{\theta 0}u^2 + k^v_{\theta 0}v^2 + k^w_{\theta 0}w^2 + K^r_{\theta 0}\phi^2_r + K^\theta_{\theta 0}\phi^2_r\right]_{\theta=0} \\ +\left[k^u_{\theta 1}u^2 + k^v_{\theta 1}v^2 + k^w_{\theta 1}w^2 + K^r_{\theta 1}\phi^2_r + K^\theta_{\theta 1}\phi^2_r\right]_{\theta=\theta_0} \end{array} \right\} dr \end{aligned} \tag{4.49d}$$

where U_s, T and W_e are the stain energy, kinetic energy and external work functions. U_{sp} represents boundary spring deformation energy function introduced by the artificial spring boundary technique (see Sect. 1.3.3 and Fig. 4.17).

The governing equations and boundary conditions for thick laminated sectorial plates are obtained by substituting Eq. (4.35) into Eqs. (1.59), (1.60) and (1.61). The governing equations are

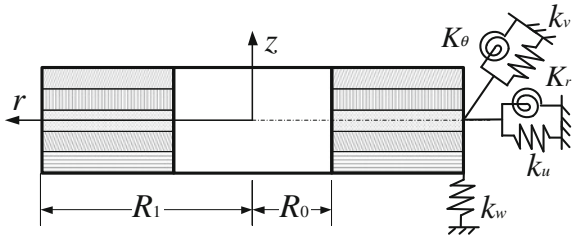

Fig. 4.17 Boundary conditions of a thick laminated sectorial plate

$$\begin{aligned}
&\frac{\partial(rN_r)}{\partial r}+\frac{\partial(N_{r\theta})}{\partial\theta}-N_\theta+rq_r=rI_0\frac{\partial^2 u}{\partial t^2}+rI_1\frac{\partial^2\phi_r}{\partial t^2}\\
&\frac{\partial(rN_{r\theta})}{\partial r}+\frac{\partial(N_\theta)}{\partial\theta}+N_{r\theta}+rq_\theta=rI_0\frac{\partial^2 v}{\partial t^2}+rI_1\frac{\partial^2\phi_\theta}{\partial t^2}\\
&\frac{\partial(rQ_r)}{\partial r}+\frac{\partial(Q_\theta)}{\partial\theta}+rq_z=rI_0\frac{\partial^2 w}{\partial t^2}\\
&\frac{\partial(rM_r)}{\partial r}+\frac{\partial(M_{r\theta})}{\partial\theta}-M_\theta-rQ_r+rm_r=rI_1\frac{\partial^2 u}{\partial t^2}+rI_2\frac{\partial^2\phi_r}{\partial t^2}\\
&\frac{\partial(rM_{r\theta})}{\partial r}+\frac{\partial(M_\theta)}{\partial\theta}+M_{r\theta}-rQ_\theta+rm_\theta=rI_1\frac{\partial^2 v}{\partial t^2}+rI_2\frac{\partial^2\phi_\theta}{\partial t^2}
\end{aligned}\tag{4.50}$$

And the corresponding boundary conditions are

$$\begin{aligned}
r=R_0:&\begin{cases}N_r-k^u_{r0}u=0\\N_{r\theta}-k^v_{r0}v=0\\Q_r-k^w_{r0}w=0\\M_r-K^r_{r0}\phi_r=0\\M_{r\theta}-K^\theta_{r0}\phi_\theta=0\end{cases}\qquad
r=R_1:\begin{cases}N_r+k^u_{r1}u=0\\N_{r\theta}+k^v_{r1}v=0\\Q_r+k^w_{r1}w=0\\M_r+K^r_{r1}\phi_r=0\\M_{r\theta}+K^\theta_{r1}\phi_\theta=0\end{cases}\\
\theta=0:&\begin{cases}N_{r\theta}-k^u_{\theta0}u=0\\N_\theta-k^v_{\theta0}v=0\\Q_\theta-k^w_{\theta0}w=0\\M_{r\theta}-K^r_{\theta0}\phi_r=0\\M_\theta-K^\theta_{\theta0}\phi_\theta=0\end{cases}\qquad
\theta=\theta_0:\begin{cases}N_{r\theta}+k^u_{\theta1}u=0\\N_\theta+k^v_{\theta1}v=0\\Q_\theta+k^w_{\theta1}w=0\\M_{r\theta}+K^r_{\theta1}\phi_r=0\\M_\theta+K^\theta_{\theta1}\phi_\theta=0\end{cases}
\end{aligned}\tag{4.51}$$

4.5 Vibration of Laminated Sectorial, Annular and Circular Plates

4.5.1 Vibration of Laminated Annular and Circular Plates

In this section, we consider free vibration of homogeneous and laminated annular and circular plates with general boundary conditions. The homogeneous circular plates are treated as special cases of the laminated ones in the studies. Only solutions considering effects of shear deformation are given in this section. The weak form solution procedure is adopted in the calculations.

There are two boundaries in an annular plate, in this work a two-letter character is employed to represent the boundary condition of an annular plate, such as FC identifies the plate with inner edge free and outer edge clamped. Unless otherwise stated, the natural frequencies of the considered plates are expressed in the non-dimensional parameters as $\Omega=\omega R_1\sqrt{\rho h/D_{11}}$. Unless otherwise stated, material

properties of the layers of laminated annular and circular plates under consideration are given as: E_2 = 10 GPa, E_1/E_2 = open, μ_{12} = 0.25, $G_{12} = 0.6E_2$, $G_{13} = 0.6E_2$, $G_{23} = 0.5E_2$ and ρ = 1,500 kg/m^3 (subscript 1 and 2 represent the principle directions of the material and they are paralleled to r and θ directions, respectively).

Considering the circumferential symmetry of annular and circular plates, each displacement and rotation component of a laminated annular or circular plate is expanded as a modified Fourier series in the following form:

$$\begin{aligned}
u(r,\theta) &= \sum_{m=0}^{M}\sum_{n=0}^{N} A_{mn}\cos\lambda_m r\cos n\theta + \sum_{l=1}^{2}\sum_{n=0}^{N} a_{ln}P_l(r)\cos n\theta \\
v(r,\theta) &= \sum_{m=0}^{M}\sum_{n=0}^{N} B_{mn}\cos\lambda_m r\ \sin n\theta + \sum_{l=1}^{2}\sum_{n=0}^{N} b_{ln}P_l(r)\sin n\theta \\
w(r,\theta) &= \sum_{m=0}^{M}\sum_{n=0}^{N} C_{mn}\cos\lambda_m r\cos n\theta + \sum_{l=1}^{2}\sum_{n=0}^{N} c_{ln}P_l(r)\cos n\theta \\
\phi_r(r,\theta) &= \sum_{m=0}^{M}\sum_{n=0}^{N} D_{mn}\cos\lambda_m r\cos n\theta + \sum_{l=1}^{2}\sum_{n=0}^{N} d_{ln}P_l(r)\cos n\theta \\
\phi_\theta(r,\theta) &= \sum_{m=0}^{M}\sum_{n=0}^{N} E_{mn}\cos\lambda_m r\ \sin n\theta + \sum_{l=1}^{2}\sum_{n=0}^{N} e_{ln}P_l(r)\sin n\theta
\end{aligned} \tag{4.52}$$

where $\lambda_m = m\pi/\Delta R$, ($\Delta R = R_1 - R_0$). n represents the circumferential wave number of the corresponding mode. It should be noted that n is non-negative integer. Interchanging of sin $n\theta$ and cos $n\theta$ in Eq. (4.52), another set of free vibration modes (anti-symmetric modes) can be obtained. P_l (r) denote the auxiliary polynomial functions introduced to remove all the discontinuities potentially associated with the first-order derivatives at the boundaries. These auxiliary functions are in the same forms as those of Eq. (4.33). Note that the modified Fourier series presented in Eq. (4.52) are complete series defined over the domain [0, ΔR]. Therefore, linear transformations for coordinates from $r \in [R_0, R_1]$ to [0, ΔR] need to be introduced for the practical programming and computing.

In Table 4.14 (Jin et al. 2014a), the first six frequencies (Hz) of a single-layered, moderately thick composite annular plate with completely free boundary conditions and different truncated configurations are chosen to demonstrate the convergence of the current method. Considering the circumferential symmetry of the annular plate, the expression terms with respect to θ in displacements and rotation components automatically satisfy the governing equations and boundary conditions. Thus, the convergence only needs to be checked in the axial direction (r). The geometric and material constants of the plate are: E_1/E_2 = 15, R_0 = 1 m, R_1 = 3 m, h = 0.1 m. In all the following computations, the zero frequencies corresponding to the rigid body modes were omitted from the results. The table shows the present solutions has fast convergence behavior.

Table 4.14 Convergence of the first six frequencies (Hz) of a single-layered composite annular plate with FF boundary conditions

$M \times N$	Mode number					
	1	2	3	4	5	6
11 × 10	7.2421	11.244	18.650	28.423	33.407	51.069
12 × 10	7.2417	11.244	18.649	28.417	33.405	51.067
13 × 10	7.2415	11.244	18.649	28.415	33.405	51.067
14 × 10	7.2414	11.244	18.648	28.413	33.404	51.066
15 × 10	7.2414	11.244	18.648	28.413	33.404	51.066

Table 4.15 Comparison of the fundamental frequency parameters Ω for composite laminated annular plates with different boundary conditions and lamination schemes ($R_0/R_1 = 0.5$)

B.C.	Method	h/R_1	Lamination schemes			
			[I]	[II]	[I/II/I/II]	[I/II/II/I]
CC	Lin and Tseng (1998)	0.10	84.977	66.057	75.706	79.226
		0.05	102.62	82.416	92.216	98.656
		0.02	110.04	89.776	99.272	107.37
		0.01	111.24	91.002	100.43	108.83
	Present	0.10	87.134	68.693	78.711	81.861
		0.05	103.58	83.591	94.013	99.876
		0.02	110.19	89.928	100.22	107.58
		0.01	111.21	90.960	101.22	108.81
SC	Lin and Tseng (1998)	0.10	76.596	54.319	65.559	71.644
		0.05	88.679	63.002	75.585	84.914
		0.02	93.307	66.337	79.362	90.250
		0.01	94.033	66.860	79.987	91.102
	Present	0.10	77.603	55.899	67.959	73.015
		0.05	89.256	63.675	77.562	85.670
		0.02	93.571	66.549	80.997	90.541
		0.01	94.189	66.994	81.528	91.265
FC	Lin and Tseng (1998)	0.10	37.329	20.636	30.173	35.010
		0.05	41.246	21.851	32.847	39.320
		0.02	42.591	22.233	33.737	40.850
		0.01	42.794	22.290	33.870	41.084
	Present	0.10	38.150	20.936	30.979	35.896
		0.05	41.582	21.995	33.371	39.689
		0.02	42.728	22.323	34.151	40.993
		0.01	42.899	22.371	34.267	41.190

To validate the accuracy and reliability of current solutions, comparison of the fundamental frequency parameters Ω for a composite laminated annular plate ($R_0/R_1 = 0.5$) when the outer edge is clamped and the inner edge is either clamped, simply supported or free is presented in Table 4.15 (Jin et al. 2014a), in which four

Table 4.16 Frequency parameters Ω of a [0°/90°] laminated circular plate with different boundary conditions ($R_1 = 1$)

h/R_1	Mode	$E_1/E_2 = 1$ (isotropic)			$E_1/E_2 = 15$		
		F	S	C	F	S	C
0.01	1	6.0186	4.8598	10.21379	3.4024	3.8685	8.8441
	2	8.8888	14.596	22.087	6.8133	8.3294	13.555
	3	13.747	27.196	36.53708	7.8292	15.542	21.015
	4	21.634	29.650	39.74355	11.828	24.076	30.300
0.05	1	5.9897	4.8524	10.16563	3.3735	3.8493	8.6463
	2	8.8615	14.525	21.86786	6.7621	8.2339	13.184
	3	13.631	26.945	35.95093	7.7342	15.230	20.229
	4	21.431	29.366	39.10696	11.630	23.360	28.832
0.1	1	5.9332	4.8295	10.01998	3.3116	3.7898	8.0874
	2	8.7785	14.311	21.22982	6.6109	7.9643	12.215
	3	13.387	26.221	34.32761	7.4922	14.397	18.329
	4	20.906	28.539	37.32406	11.107	21.526	25.448

different thickness-radius ratios are included, i.e., $h/R_1 = 0.1$, 0.05, 0.02 and 0.01, corresponding to thick to thin laminated annular plates. Four types of lamination schemes included in the comparison are: [I], [II], [I/II/I/II] and [I/II /II/I], where I and II represent two kinds of composite laminate, their material properties are given as: for material I: $E_2/E_1 = 50$, $G_{12} = 0.6613E_1$, $G_{13} = G_{23} = 0.5511E_1$, $\mu_{12} = 0.006$; for material II: $E_2/E_1 = 5$, $G_{12} = 0.35E_1$, $G_{13} = G_{23} = 0.292E_1$, $\mu_{12} = 0.06$. By comparing, we can find that the discrepancies between present results and solutions reported by Lin and Tseng (1998) based on an eight node isoparametric finite element method are acceptable. The discrepancy in the results may be attributed to different solution approaches are used in the literature. The table also shows that natural frequencies are influenced by stacking sequence, the order of the magnitude of the fundamental frequencies for the four different lamination schemes being [I] > [I/II/II/I] > [I/II/I/II] > [II].

For a circular plate, there is only one boundary. Table 4.16 shows the lowest three frequency parameters Ω for a [0°/90°] laminated circular plate with different boundary conditions and thickness-to-outer radius ratios (h/R_1). The F, S and C boundary conditions, two orthotropy ratio $E_1/E_2 = 1$ and 25, and thickness-to-outer radius ratios of 0.01, 0.05 and 0.1 are used. As seen in the table, the frequency parameters for the circular plate with $E_1/E_2 = 25$ are smaller than those of $E_1/E_2 = 1$. And the frequency parameters decrease with the thickness-to-outer radius ratio increases. The corresponding contour mode shapes for the plate with orthotropy ratio $E_1/E_2 = 25$ and thickness-to-outer radius ratios $h/R_1 = 0.05$ are given in Fig. 4.18. As seen in the figure, the mode shapes for S boundary conditions are similar to those of C boundary conditions.

Table 4.17 presents the first three frequency parameters Ω of a [0°/90°] laminated annular plate with different boundary conditions and various inner-to-outer

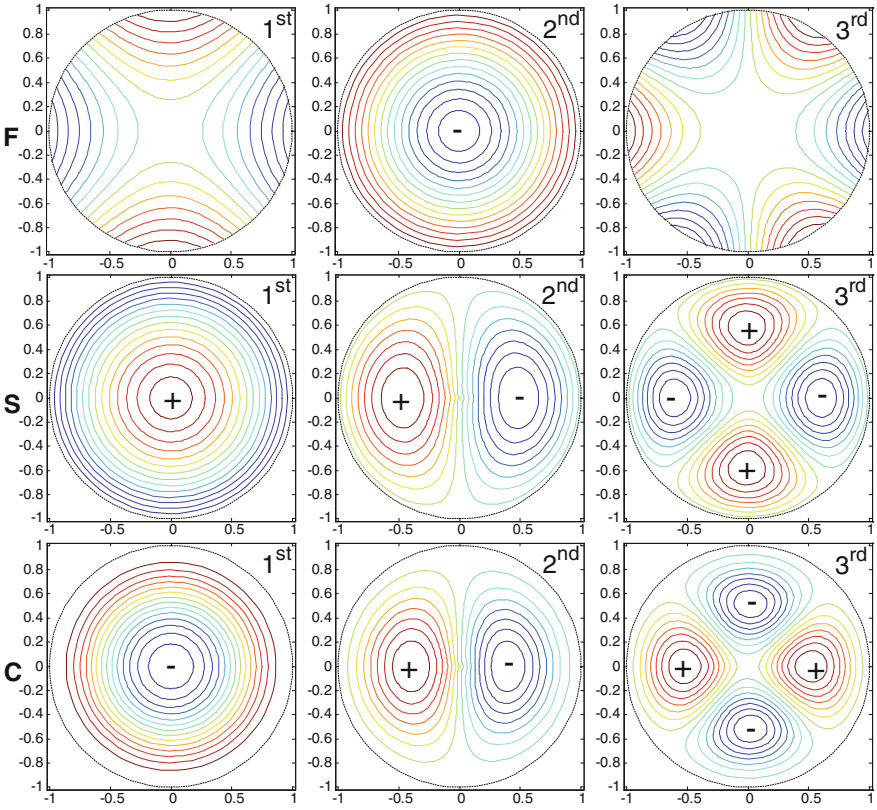

Fig. 4.18 Mode shapes for a [0°/90°] laminated circular plate with different boundary conditions ($h/R_1 = 0.05$, $E_1/E_2 = 15$)

radius ratios (R_0/R_1). The considered plate is assumed to be made of composite layers with following parameters: $R_1 = 1$, $h/\Delta R = 0.05$, $E_1/E_2 = 15$. Four inner-to-outer radius ratios, i.e., $R_0/R_1 = 0.2$, 0.4, 0.6 and 0.8 and six sets of boundary conditions, i.e., FF, FS, FC, SS, SC and CC are studied. From the table, we can see that frequency parameters for the plate with FC, SS, SC and CC boundary conditions increase with inner-to-outer radius ratio increases. However, for FF boundary conditions, the maximum fundamental, second and third frequency parameters occur at inner-to-outer radius ratios of 0.2, 0.6 and 0.8, respectively and for FS boundary conditions, the minimum fundamental, second and third frequency parameters separately occur at inner-to-outer radius ratios of 0.2, 0.4 and 0.8, respectively. In order to enhance our understanding of the effects of the inner-to-outer radius ratios on vibrations of annular plates, the lowest three mode shapes for the laminated annular plate with FC boundary conditions are given in Fig. 4.19. Due to the circumferential symmetry of the annular plate, the mode shapes are symmetrical as well. These figures also show that mode shapes are influenced by

Table 4.17 The first three frequency parameters Ω of a [0°/90°] laminated annular plate with different boundary conditions ($R_1 = 1$, $h/\Delta R = 0.05$, $E_1/E_2 = 15$)

R_0/R_1	Mode	Boundary conditions					
		FF	FS	FC	SS	SC	CC
0.2	1	3.1899	3.5483	9.3364	14.912	20.177	23.162
	2	5.4501	7.7562	12.451	15.777	20.824	24.238
	3	7.7137	14.481	19.806	17.211	22.320	24.421
0.4	1	2.8314	4.0587	12.171	25.444	32.994	40.389
	2	5.6991	6.9513	12.853	25.519	33.033	40.637
	3	7.4366	13.351	18.527	26.532	33.932	40.768
0.6	1	2.4299	5.4710	20.153	55.144	69.808	88.976
	2	6.7767	7.5738	20.301	55.323	69.963	89.035
	3	7.1894	12.736	22.748	56.113	70.660	89.392
0.8	1	2.0330	9.8049	64.064	215.18	268.65	351.93
	2	5.8389	12.098	64.184	215.40	268.85	352.06
	3	11.255	17.545	65.209	216.10	269.49	352.47

inner radius. Figure 4.20 shows the lowest three mode shapes for the laminated annular plate ($R_0/R_1 = 0.4$) with CF and FC boundary conditions. It can be seen that the mode shapes of the plate in these two cases are quite different although the plate is camped at one boundary and free at the other boundary.

4.5.2 Vibration of Laminated Sectorial Plates

In this section, we consider free vibration of laminated sectorial plates with general boundary conditions. Similar to the studies performed earlier for laminated annular and circular plates, the results given in this section are obtained by using the shear deformation plate theory (SDPT) and weak form solution procedure. Only plates having polar orthotropy will be studied.

For a general sectorial plate, there exist four boundaries, i.e., $r = R_0$, $r = R_1$, $\theta = 0$ and $\theta = \theta_0$. For the sake of brevity, a four-letter character is employed to represent the boundary condition of a sectorial plate, such as FCSC identifies the plate with F, C, S and C boundary conditions at boundaries $r = R_0$, $\theta = 0$, $r = R_1$ and $\theta = \theta_0$, respectively. In addition, unless otherwise stated, the non-dimensional frequency parameter $\Omega = \omega R_1 \sqrt{\rho h / D_{11}}$ is used and material properties of the layers of laminated sectorial plates under consideration are given as: E_2 = 10 GPa, $E_1/E_2 =$ open, $\mu_{12} = 0.25$, $G_{12} = 0.6E_2$, $G_{13} = 0.6E_2$, $G_{23} = 0.5E_2$ and $\rho = 1{,}500$ kg/m^3.

For a circular or annular plate, the assumed 2D displacement field can be reduced to a quasi 1D problem through Fourier decomposition of the circumferential wave motion. However, for a general sectorial plate, the assumption of whole periodic wave numbers in the circumferential direction is inappropriate, and thus, a

set of complete two-dimensional analysis is required and resort must be made to a full two-dimensional solution scheme. Therefore, each displacement and rotation component of the laminated sectorial plates is expanded as a two-dimensional modified Fourier series as:

$$\begin{aligned}
u(r,\theta) &= \sum_{m=0}^{M}\sum_{n=0}^{N} A_{mn}\cos\lambda_m r\cos\lambda_n\theta + \sum_{l=1}^{2}\sum_{n=0}^{N} a_{ln}P_l(r)\cos\lambda_n\theta \\
&\quad + \sum_{l=1}^{2}\sum_{m=0}^{M} b_{lm}P_l(\theta)\cos\lambda_m r \\
v(r,\theta) &= \sum_{m=0}^{M}\sum_{n=0}^{N} B_{mn}\cos\lambda_m r\cos\lambda_n\theta + \sum_{l=1}^{2}\sum_{n=0}^{N} c_{ln}P_l(r)\cos\lambda_n\theta \\
&\quad + \sum_{l=1}^{2}\sum_{m=0}^{M} d_{lm}P_l(\theta)\cos\lambda_m r \\
w(r,\theta) &= \sum_{m=0}^{M}\sum_{n=0}^{N} C_{mn}\cos\lambda_m r\cos\lambda_n\theta + \sum_{l=1}^{2}\sum_{n=0}^{N} e_{ln}P_l(r)\cos\lambda_n\theta \\
&\quad + \sum_{l=1}^{2}\sum_{m=0}^{M} f_{lm}P_l(\theta)\cos\lambda_m r \\
\phi_r(r,\theta) &= \sum_{m=0}^{M}\sum_{n=0}^{N} D_{mn}\cos\lambda_m r\ cos\lambda_n\theta + \sum_{l=1}^{2}\sum_{n=0}^{N} g_{ln}P_l(r)\cos\lambda_n\theta \\
&\quad + \sum_{l=1}^{2}\sum_{m=0}^{M} h_{lm}P_l(\theta)\cos\lambda_m r \\
\phi_\theta(r,\theta) &= \sum_{m=0}^{M}\sum_{n=0}^{N} E_{mn}\cos\lambda_m r\ cos\lambda_n\theta + \sum_{l=1}^{2}\sum_{n=0}^{N} i_{ln}P_l(r)\cos\lambda_n\theta \\
&\quad + \sum_{l=1}^{2}\sum_{m=0}^{M} j_{lm}P_l(\theta)\cos\lambda_m r
\end{aligned} \tag{4.53}$$

where $\lambda_m = m\pi/\Delta R$ and $\lambda_n = n\pi/\theta_0$. $P_l\,(r)$ and $P_l\,(\theta)$ denote the auxiliary polynomial functions introduced to remove all the discontinuities potentially associated with the first-order derivatives at the boundaries. These auxiliary functions are in the same form as those of Eq. (4.33). Similarly, linear transformations for coordinates from $r \in [R_0, R_1]$ to $[0, \Delta R]$ need to be introduced for the practical programming and computing.

Table 4.18 shows a convergence and comparison study of the lowest six natural frequencies (Hz) for an isotropic (E = 210 GPa, μ = 0.3 and ρ = 7,800 kg/m^3) sectorial plate with FFFF and CCCC boundary conditions. The sectorial plate having inner radius R_0 = 0.5 m, outer radius R_1 = 1 m, thickness h = 0.01 m and circumferential dimension $\theta_0 = \pi$. The present results are compared with those of

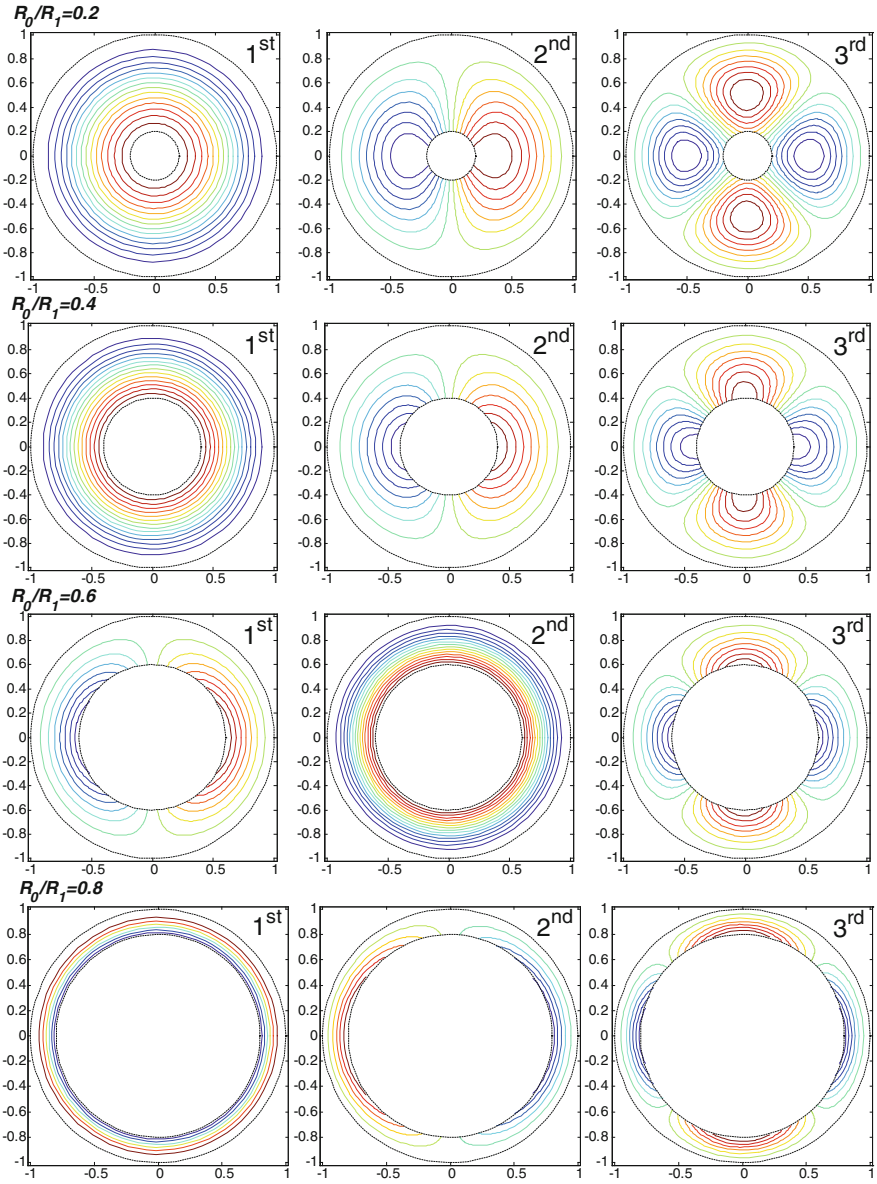

Fig. 4.19 Mode shapes for a [0°/90°] laminated annular plate with FC boundary conditions

FEM analysis (ANSYS with element type of SHELL63 and element size of 0.01 m). As can be seen from Table 4.18, the frequencies have converged monotonically up to four significant figures as the truncation numbers increase. The table also shows good agreements in the comparison.

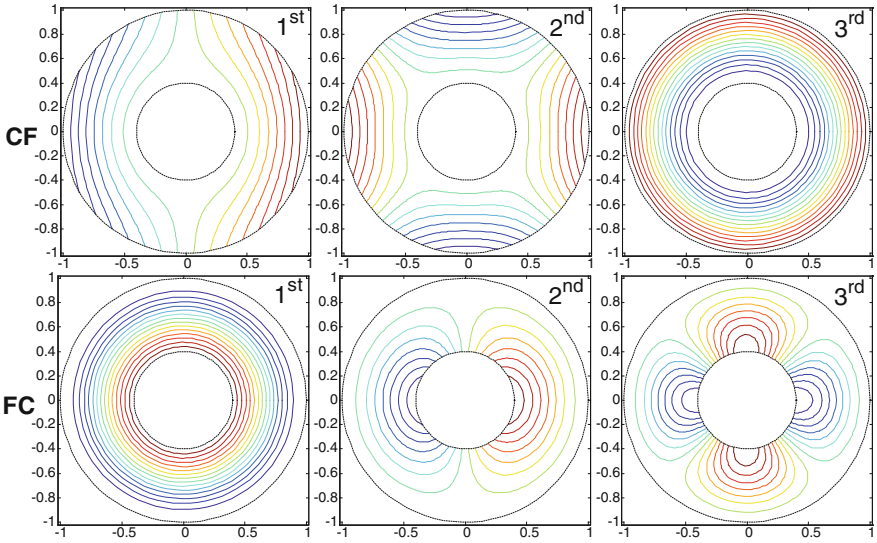

Fig. 4.20 Mode shapes for a [0°/90°] laminated annular plate (R_0/R_1 = 0.4) with CF and FC boundary conditions

Table 4.18 Convergence and comparison of frequencies (Hz) for an isotropic sectorial plate with FFFF and CCCC boundary conditions (R_0 = 0.5 m, R_1/R_0 = 2, h/R_0 = 0.02, $\theta_0 = \pi$, E = 210 GPa, μ = 0.3 and ρ = 7,800 kg/m^3)

Boundary conditions	$M \times N$	Mode number					
		1	2	3	4	5	6
FFFF	15 × 15	17.775	18.739	38.540	42.003	69.740	71.841
	15 × 16	17.760	18.738	38.537	41.999	69.706	71.838
	15 × 17	17.757	18.736	38.537	41.990	69.699	71.833
	15 × 18	17.747	18.735	38.535	41.988	69.683	71.831
	16 × 18	17.742	18.733	38.524	41.983	69.677	71.810
	17 × 18	17.739	18.730	38.520	41.982	69.675	71.807
	18 × 18	17.735	18.728	38.510	41.979	69.670	71.790
	ANSYS	17.744	18.729	38.677	42.006	69.741	72.094
CCCC	15 × 15	225.33	234.63	251.37	276.82	311.91	357.42
	15 × 16	225.33	234.62	251.32	276.67	311.73	356.71
	15 × 17	225.33	234.60	251.27	276.59	311.47	356.47
	15 × 18	225.32	234.59	251.24	276.51	311.36	356.08
	16 × 18	225.31	234.57	251.23	276.49	311.34	356.06
	17 × 18	225.31	234.57	251.22	276.48	311.33	356.06
	18 × 18	225.30	234.56	251.21	276.47	311.32	356.05
	ANSYS	225.97	235.24	251.88	277.09	311.76	356.24

Table 4.19 The first five frequency parameters Ω of a [0°/90°] laminated sectorial plate with different boundary conditions (R_0 = 0.5 m, R_1/R_0 = 2, $\theta_0 = \pi$, E_1/E_2 = 15)

$h/\Delta R$	Mode	Boundary conditions					
		FFFF	SSSS	CCCC	FCFC	CFCF	FSFS
0.01	1	3.9802	36.096	59.994	2.0332	59.062	2.6844
	2	4.7963	37.086	60.694	5.1950	59.126	7.2936
	3	8.3330	39.772	62.835	10.284	60.041	9.6338
	4	10.548	44.802	67.063	10.993	61.283	13.394
	5	14.906	52.593	73.970	17.032	64.075	16.789
0.05	1	3.9119	36.015	57.657	2.0275	56.796	2.6443
	2	4.7635	36.981	58.354	5.1583	56.856	7.2195
	3	8.2257	39.587	60.436	10.177	57.697	9.5120
	4	10.460	44.442	64.528	10.863	58.893	13.241
	5	14.652	51.929	71.121	16.809	61.577	16.524
0.10	1	3.8324	34.360	51.823	2.0151	51.149	2.6109
	2	4.7117	35.297	52.512	5.0908	51.204	7.1182
	3	8.0639	37.800	54.508	9.9678	51.872	9.3185
	4	10.292	42.399	58.366	10.579	53.000	12.974
	5	14.162	49.357	64.439	16.332	55.494	15.953

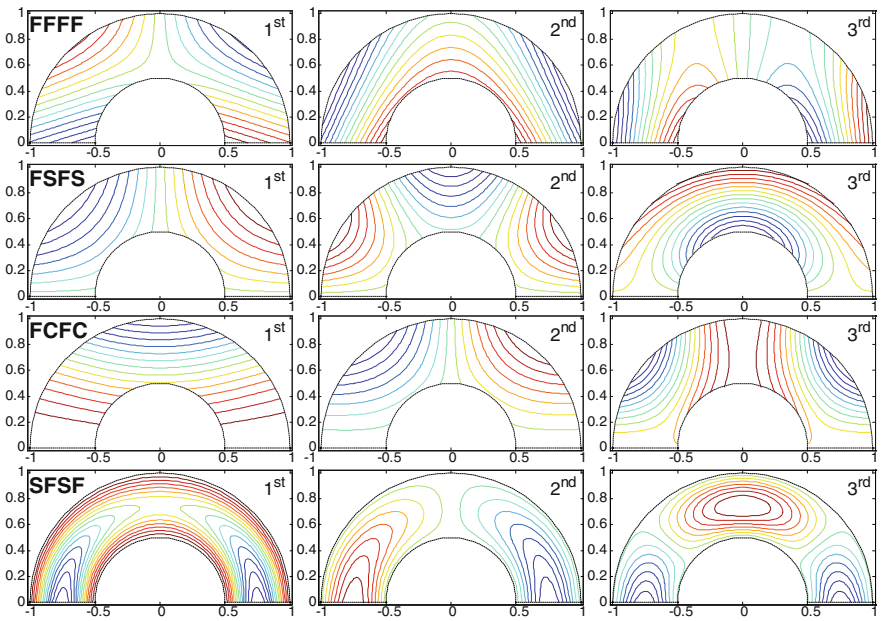

Fig. 4.21 Mode shapes for a [0°/90°] laminated sectorial plate (R_0/R_1 = 0.5, $h/\Delta R$ = 0.05) with various boundary conditions

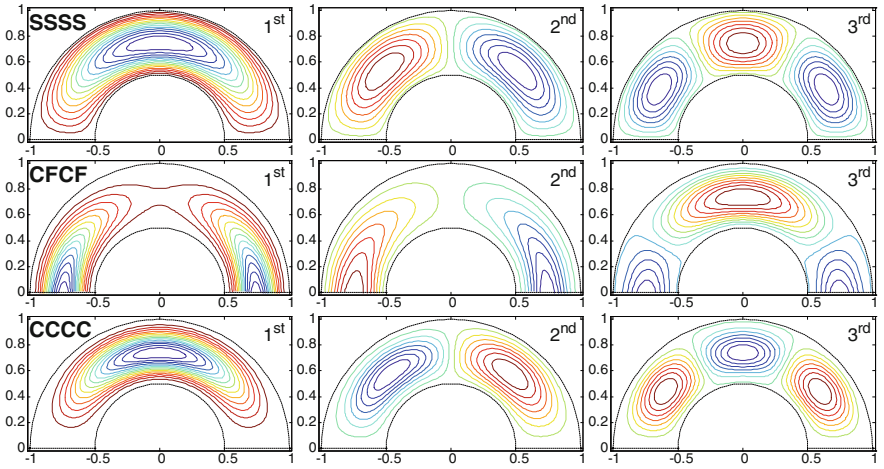

Fig. 4.21 (continued)

The effects of thickness ratio ($h/\Delta R$) on the frequency parameters of sectorial plates are studied by the following example. Table 4.19 shows the lowest five frequency parameters Ω for a [0°/90°] laminated sectorial plate with different boundary conditions and various thickness ratios $h/\Delta R$. The sectorial plate is assume to be made of polar orthotropic layer of orthotropy ratio $E_1/E_2 = 15$. Three types of thickness ratios, i.e., $h/\Delta R = 0.01$, 0.05 and 0.1, corresponding to thin to moderately thick sectorial plates are considered in the investigation. From the table, we can see that the frequency parameters of the plate in all cases decrease with the thickness ratio $h/\Delta R$ increases. Despite this, it should be noted that, the natural frequencies of the plate increase with the thickness ratio $h/\Delta R$ increases due to the fact that the stiffness of the plate get larger. The corresponding contour mode shapes for the plate with thickness ratio $h/\Delta R = 0.05$ are given in Fig. 4.21 as well. As seen in the figure, the mode shapes for the SSSS boundary conditions are similar to those for boundary conditions of CCCC. Due to the symmetry in the boundary conditions and geometry, the corresponding mode shapes of the plate are symmetrical as well.

The effects of circumferential dimension (i.e., circumferential included angle θ_0) on the frequency parameters of sectorial plates are also investigated. Table 4.20 shows the lowest five frequency parameters Ω for a [0°/90°] laminated sectorial plate with different boundary conditions and circumferential dimensions. The geometry and material parameters of the considered sectorial plate are similar to those used in Table 4.20 except that the current plate having a thickness-to-inner radius ratio $h/\Delta R = 0.1$. From the table, we can see that the fundamental frequency parameter of the plate having CFFF boundary conditions increases with circumferential included angle θ_0 increases while for the plate with CCCF boundary

Table 4.20 The first five frequency parameters Ω of a [0°/90°] laminated sectorial plate with different boundary conditions and circumferential dimensions (R_0 = 0.5 m, R_1/R_0 = 2, h/R_0 = 0.1, E_1/E_2 = 15)

θ_0	Mode	Boundary conditions					
		FFFC	FFCC	FCCC	CFFF	CCFF	CCCF
π/4	1	6.3800	18.779	56.096	7.4494	10.329	52.191
	2	15.500	57.237	86.414	10.749	29.959	69.542
	3	30.226	61.331	108.72	32.499	51.239	115.45
	4	43.421	94.202	149.20	33.550	69.149	123.79
	5	58.385	114.59	151.39	48.868	75.023	137.53
3π/4	1	0.8700	12.794	17.871	7.9348	8.0795	51.175
	2	2.5360	18.789	27.405	8.0873	9.2724	52.190
	3	6.1158	28.739	41.720	9.3391	12.500	54.578
	4	9.4626	42.736	58.147	13.085	19.445	60.033
	5	10.027	56.919	61.123	20.115	29.359	69.307
5π/4	1	0.3527	12.685	15.313	7.9946	8.0151	51.179
	2	0.8757	15.430	17.926	8.0296	8.7689	51.749
	3	2.5561	18.667	23.342	8.7377	9.2431	52.120
	4	4.6200	24.160	30.564	8.9771	10.502	53.205
	5	4.9623	31.311	39.131	10.708	13.310	55.254

conditions, the minimum fundamental frequency parameter occurs at $\theta_0 = 3\pi/4$. In other cases, the frequency parameters decrease with circumferential included angle θ_0 increases. This may be attributed to the stiffness of the sectorial plate reduce with circumferential included angle θ_0 increases.

For a solid sectorial plate, there exist only three boundaries, i.e., $r = R_1$, $\theta = 0$ and $\theta = \theta_0$. The results on this subject are very limited in the open literature. The lowest three frequency parameters and contour plots of the corresponding mode shapes for a [0°/90°] laminated solid sectorial plate are given in Fig. 4.22. The orthotropy ratio is chosen to be E_1/E_2 = 15. The thickness ratio h/R_1 = 0.05 is used in the calculation. The circumferential included angle θ_0 is varied from π/2 (90°) to 3π/2 (270°) by a step of π/4 (45°). The solid laminated sectorial is completely clamped (C) at boundary $r = R_1$ and completely free (F) at the other two boundaries. It is noticed that vary θ_0 from π/2 to 3π/2 increases the fundamental frequency parameter of the plate. For the second mode, it can be found that the minimum frequency parameter occurs at $\theta_0 = 5\pi/4$. Considering the third mode, it is observed that increasing θ_0 from π/2 to 3π/2 decreases the value of the frequency parameter. In addition, the mode shapes in all the subfigures are symmetrical about geometric center line. It is attributed to the symmetry in the boundary conditions and geometry of the plate. The similar observations can be seen in Figs. 4.18, 4.19, 4.20 and 4.21 as well.

In conclusion, vibration of laminated plates is studied in this chapter, including the rectangular, circular, annular and sectorial plates. A variety of vibration results including frequencies and mode shapes for laminated plates with classical and

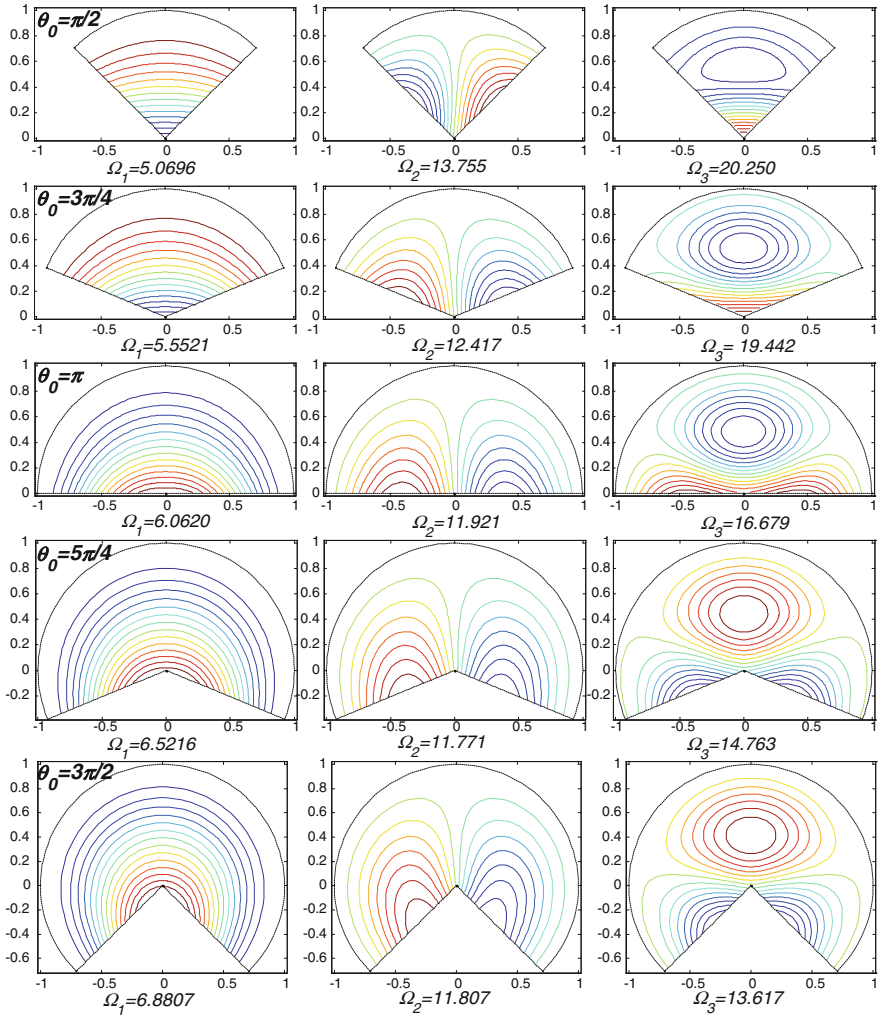

Fig. 4.22 Mode shapes and frequency parameters for a [0°/90°] laminated solid sectorial plate with various circumferential dimensions ($R_1 = 1$, $h/R_1 = 0.05$, $E_1/E_2 = 15$)

elastic boundary conditions are presented for different geometric and material parameters and lamination schemes, which may serve as benchmark solution for future researches. It is found that due to the symmetry in the boundary conditions and geometry, mode shapes of the annular and circular plates are symmetrical as well.